

Processing methods for making porous bioactive glass-based scaffolds—A state-of-the-art review

*Original*

Processing methods for making porous bioactive glass-based scaffolds—A state-of-the-art review / Baino, F., Fiume, E., Barberi, J., Kargozar, S., Marchi, J., Massera, J., Verne, E.. - In: INTERNATIONAL JOURNAL OF APPLIED CERAMIC TECHNOLOGY. - ISSN 1546-542X. - ELETTRONICO. - 16:5(2019), pp. 1762-1796. [10.1111/ijac.13195]

*Availability:*

This version is available at: 11583/2766415 since: 2023-04-20T08:18:40Z

*Publisher:*

Blackwell Publishing Ltd

*Published*

DOI:10.1111/ijac.13195

*Terms of use:*

This article is made available under terms and conditions as specified in the corresponding bibliographic description in the repository

*Publisher copyright*

(Article begins on next page)

Article type: Special Issue Article

Corresponding author mail id :francesco.baino@polito.it

**Processing methods for making porous bioactive glass-based scaffolds – a state-of-the-art review**

Francesco Baino<sup>1,\*a</sup>, Elisa Fiume<sup>1</sup>, Jacopo Barberi<sup>1</sup>, Saeid Kargozar<sup>2</sup>, Juliana Marchi<sup>3</sup>, Jonathan Massera<sup>4,a</sup>, Enrica Verné<sup>1,a</sup>

<sup>1</sup> Institute of Materials Physics and Engineering, Department of Applied Science and Technology, Politecnico di Torino, Torino, Italy

<sup>2</sup> Department of Modern Sciences and Technologies, School of Medicine, Mashhad University of Medical Sciences, Mashhad, Iran

<sup>3</sup> Center for Natural Sciences and Humanities, Federal University do ABC, Santo André, Brazil

<sup>4</sup> Faculty of Medicine and Health Technology, Tampere University, Tampere, Finland

<sup>a</sup> Member of the American Ceramic Society (ACerS)

This article has been accepted for publication and undergone full peer review but has not been through the copyediting, typesetting, pagination and proofreading process, which may lead to differences between this version and the Version of Record. Please cite this article as doi: 10.1111/ijac.13195

This article is protected by copyright. All rights reserved.

## Abstract

Bioactive glasses exhibit the unique ability of bone bonding, thus creating a stable interface by stimulating bone cells towards mechanisms of regeneration and self-repair activated by ionic dissolution products. Therefore, 3D glass-derived scaffolds can be considered ideal porous templates to be used in bone tissue engineering strategies and regenerative medicine. This review provides a comprehensive overview of all technological aspects relevant to the fabrication of bioactive glass scaffolds, including the fundamentals of materials processing, a summary of the conventional porogen and template-based methods and of recent additive manufacturing technologies, which are promising for large-scale production of highly reproducible and reliable implants suitable for a wide range of clinical applications.

**Keywords:** Bioactive glasses; Bioceramics; Scaffolds; Additive manufacturing.

## 1. INTRODUCTION

Worldwide, osteoporosis causes more than 8.9 million fractures annually, resulting in an osteoporotic fracture every 3 seconds [1], needing bone regeneration process. Besides osteoporosis, bone cancer and pathologies related to old-age people deserves great attention.

If bone is affected by self-repairing incompetence, modern surgery offers many different therapeutic/operative approaches that a surgeon can choose, depending on the type of bone involved, the characteristics of the damage and the age and health of the patient [2]–[4]. In case of a fracture or trauma without the loss of bone material, osteosynthesis devices such as bone screws or intramedullary rods can be implanted [5].

In the case of critical tissue defects due to tumor removal, big trauma or distraction osteogenesis (i.e. a surgical technique that allows extending or modifying the shape of the bone through an osteotomy and controlled distraction of the bone segments) [6], bone

may be not able to self-heal spontaneously, thus requiring what is called bone grafting. The surgeon transplants or implants new natural or man-made material, respectively, in the defect site in order to help the natural healing process of the bone. An ideal material for bone grafting should promote osteogenesis, osteointegration, osteoconductivity or even osteoinductivity [7], defined as follows.

- Osteogenesis is the ability to differentiate osteoblasts from the osteoprogenitor cells present in the bone or in the grafting material (if previously seeded with cells) in order to produce new bone;
- Osteointegration is the ability to create a stable chemical bond with the physiological tissue avoiding the formation of a fibrous layer;
- Osteoconductivity is the ability to support the new tissue growth at the graft-tissue interface, thus determining the formation of an oriented and well-organized vascularization and new Haversian systems;
- Osteoinductivity is the ability of the material to induce the production of bone-forming cells via differentiation of multipotent mesenchymal stem cells. These cells are located in the surrounding tissue and can produce osteoprogenitor cells [8], [9].

The use of synthetic implantable materials is of great importance due to the current limitations in the transplantation of natural bone tissue from human or animal origin (i.e. auto-, allo-, and xeno-grafts), including donor shortage, risk of immunological rejection and infection transition, and ethical/religious concerns [10],[11].

Man-made biomaterials are available in the form of monolithic pieces, granules or porous scaffolds, defined as three-dimensional devices able to mimic the bone structure and to stimulate the restoration processes of the healthy bone. These implants are typically made of hydroxyapatite (HA) and other calcium phosphates, bioactive glasses and glass-ceramics, or polymer-based composites [12].

An ideal scaffold aimed at repairing bone should satisfy some requirements, including mechanical properties matching those of host bone and positive interaction with the biological environment of the damaged bone [13].

Bone substitute scaffolds can be (almost) permanent or bioresorbable. The first one is made of those materials requiring very long time (around years) to dissolve (e.g. HA [14]) or remaining indefinitely in the fracture site, just being embedded in the newly-formed bone. On the contrary, the second type is composed by biodegradable material that will be progressively resorbed over time, thus leaving space to the new bone to grow and self-remodel. In this case, degradation kinetics and, hence, the loss of mechanical properties over time should be carefully taken into account, especially in load-bearing applications [15].

Bioactive glass-based scaffolds can be permanent or biodegradable depending on their formulation [16]. There are three main classes of biomedical glasses that are used in the fabrication of scaffolds, sorted by their former oxide.

1. Silicate-based glasses, including the well-known 45S5 Bioglass<sup>®</sup> (45SiO<sub>2</sub>-24.5CaO-24.5Na<sub>2</sub>O-6P<sub>2</sub>O<sub>5</sub> wt.%), developed by Hench and coworkers in 1969 [17] and commercialized over the years in different forms for applications in orthopedic and dentistry (e.g. cast blocks, granules, fine particulate) [18].
2. Borate-based glasses, which have greatly attracted researchers' interest since the late 2000s for their higher reactivity in contact with biological fluids, compared to silicate-based ones, and, hence, a faster rate of conversion to HA [19].
3. Phosphate-based glasses, which exhibit a great tendency to spontaneously dissolve in aqueous media and are therefore ideal materials to fabricate temporary implants [20]; furthermore, these glasses can be also drawn in fibers to produce mats or conduits for muscle tissue engineering [21] and peripheral nerve regeneration [22].

In addition to the former oxides and basic modifiers (e.g. CaO, Na<sub>2</sub>O), a lot of other metallic doping elements can be added to the composition to tune the bioactivity and give peculiar extra-functionalities to the glasses, such as silver (antibacterial effect), copper (angiogenesis) and strontium (anti-osteoporotic effect) [10], [23]–[26].

Combining different kinds of materials is a valuable strategy to obtain new materials with enhanced properties, resulting from the characteristics of the starting raw materials. Thus, it is possible to finely design and improve the physico-chemical and mechanical properties of the final scaffold by merging polymers and bioactive glasses [27]. One of the major problems of using bioactive glasses is their intrinsic fragility, as they are non-crystalline brittle ceramic materials undergoing catastrophic failure, which is further emphasized by the presence of pores [28]. Depositing a polymeric coating on a porous glass or glass-ceramic scaffold is an effective way to increase toughness. On the other hand, glass fillers embedded in a polymeric matrix have the effects of improving stiffness and mechanical strength of the composite [27]. Furthermore, biological and chemical advantages can be obtained: for example, as polymers release acid residues upon their degradation that could provoke inflammatory responses *in vivo*, glass inclusions can locally increase the pH of the fluids during their dissolution, thus they can contrast and buffer the effects of the polymer resorption by releasing alkaline ionic species. This interesting buffering property has been recently exploited to fabricate polymer/glass “soft” patches for cardiac tissue engineering [29]. Furthermore, release of ions from the bioactive glass inclusions can confer bioactive properties to polymers that are only biodegradable.

## **2. MAJOR FEATURES AND PROPERTIES FOR A PROPER SCAFFOLD DESIGN**

Since the aim of a scaffold is to substitute the damaged bone, as well as to guide and increase the healing process of the surrounding bone, it has to be as much similar as possible to the structure of healthy bone. Therefore, the manufacturing process and the biomaterials employed should be carefully selected in order to obtain the desired properties. Furthermore, the scaffold should be obtainable in a large variety of shapes and dimensions to fit the size of the defect and at a reasonable cost for the patients. Last but not least, before being implanted, the scaffold should sustain the sterilization process without modifying its original characteristics. The general suitable features of a porous scaffold for tissue engineering are summarized in **Table 1**.

In the next sections, some important features that should be taken into account in the development of a bone tissue engineering scaffold are discussed.

### **2.1. Biocompatibility**

Since the 3D scaffold will be placed inside the human body, it should have the ability to stimulate an appropriate response from the surrounding biological environment without inducing any potentially toxic effect, either local or systemic. In the medical field, this firstly means that the scaffold should not elicit a foreign body reaction (FBR). When a prosthetic material is implanted inside the human body, the first thing that happens is the adsorption of water molecules and proteins. Then, macrophages try to dismantle the foreign device but, being unsuccessful in doing it immediately, fuse together and form giant cells in the attempt to eliminate or isolate the external body. The giant cells secrete cytokines (a protein signaling agent) that allow fibroblasts to be recruited on site. As a consequence, fibroblasts produce collagen for encasing the biomaterial into an acellular collagenous capsule that, after being formed in 4-8 weeks, may lead to prosthesis loosening and/or rejection of the implant [30].

On the contrary, an ideal biomaterial for bone tissue engineering scaffolds should tightly bond bone and promote new bone growth.

In the case of biodegradable scaffolds, the disposal and removal of the degradation by-products should be carefully studied. An accumulation of the ionic dissolution species could trigger an inflammatory local response as the metabolic activity and the vascularization are poor in the tissues surrounding the scaffold, thus reducing the elimination ability of the scaffolds by-products [31], [32]. A comprehensive overview of the *in vivo* effects elicited by bioactive glass scaffolds has been recently reported elsewhere [33].

## **2.2. Hierarchical structure and porosity**

The human bone has a very complex structure on different dimensional levels, from the nanoscale to the macroscale [34]. In the cortical bone, there are small vascular channels and canaliculi in the range of 1 to 5  $\mu\text{m}$ , Volkmann's canals and osteocyte lacunae within 5-15  $\mu\text{m}$ , and Haversian canals up to 100  $\mu\text{m}$  [35]. Since the scaffold should act as a template for the physiological growth of the newly-formed bone, it should have peculiar features at different dimensional ranges, mimicking the hierarchical structure of natural bone. This means that an accurate design, combined with a suitable manufacturing process, should lead to a highly porous scaffold (about 80 vol.%) with interconnected pores ranging from 300  $\mu\text{m}$  to less than 10  $\mu\text{m}$ . In fact, it has been shown that interconnected pores with size under 100  $\mu\text{m}$  lead to a poor vascularization for the area and to hypoxic growth conditions; hence, not only mineralized bone but also cartilage will form [36]. On the other hand, larger pores (above 200-300  $\mu\text{m}$ ) enhance the vascularization process and, therefore, to the formation of new mineralized bone [36]. The disadvantage of large pores is that they negatively affect the mechanical strength of scaffolds; however, the presence of pores is useful to decrease the

high Young's modulus of bioactive ceramic and glass implants to values closer to those of trabecular bone, thereby avoiding problems of stress shielding and stiffness mismatch.

Even larger pores, with milli-metric dimension, can be introduced as suture anchoring points for surgical fixation. Along with macro-porosity, also micro-porosity is needed. Pores between 2 and 10  $\mu\text{m}$  enhance the specific surface area of the scaffold, increasing protein adsorption, cell adhesion, diffusion of nutrients and removal of waste products [36]. A porous structure on the scaffold surface (surface roughness) can also increase the mechanical interlocking with the surrounding bone ensuring a better load transfer and avoiding the loosening of the implant.

### 2.3. Mechanical properties

Since the scaffold has to act as a bone substitute during new bone formation, it may have to withstand mechanical loads, especially if the implant is surgically placed in a load-bearing location. Scaffolds strength and stiffness have to be properly balanced in order to ensure both mechanical integrity upon physiological activities and a correct load transfer to the surrounding tissue avoiding resorption. This task is not so easy to get, because each bone site in the human body is subject to very different stimuli, so the mechanical properties of the scaffold should be customizable with respect to each specific application, implantation site, age, lifestyle and health of the patient.

Despite the intrinsic brittleness of ceramic scaffolds, resulting from the fabrication process that leads to the presence of defects and micro-pores also in the solid fraction, several research groups were successful in producing glass scaffolds showing comparable mechanical properties to that of the human bone [16], as shown in **Figure 1**.

For example, high mechanical properties can be obtained by producing anisotropic scaffolds with a clear orientation of the pores. Such orientation is quite easily achievable by solid

freeform fabrication and unidirectional freezing of suspensions. Moreover, while flexural strength usually matches that of the trabecular bone in some scaffolds, almost none of them was as strong as the cortical one [16].

Another property that deserves attention is the fracture toughness of the scaffolds. Due to its fragile-ductile composite structure, human bones are very tough materials, with the ability to raise the fracture toughness by means of crack deflection, organic bridging between mineral domains and micro-cracking [37]. Moreover, bone has the unique ability to repair the cracks, always restoring its properties. In order to use scaffolds as a bone substitute in load bearing areas, their toughness must be controlled in order to achieve suitable values. Scaffolds have been toughened by several approaches. For example, Peroglio *et al.* [37] improved the mechanical properties of a biphasic HA/ $\beta$ TCP scaffolds by infiltrating it with poly( $\epsilon$ -caprolactone), thus coating the internal structure of the scaffolds. In this way, crack-bridging performed by polymeric fibrils was reported to be the main toughening mechanism [37]. This approach was found very suitable to significantly improve the tensile strength of 45S5 Bioglass<sup>®</sup> scaffolds from 0.01 to 0.07 MPa. However, this result is still far from the strength of natural bone (2-20 MPa for human femoral spongy bone [38]), thus suggesting further improvements.

#### **2.4. Surface properties**

The surface of the scaffold is the main site where the first interaction between the biomaterial and the human body takes place. Surface characteristics are known to have a remarkable effect on cell adhesion and tissue response to biomedical implants [39]–[41]. Immediately after the implantation, the scaffold comes into contact with biological fluids. As soon as the biomaterial is placed into the body, a layer of adsorbed water forms on the implant surface. Then, proteins interact with water and are quickly adsorbed on the surface [42]. According to

the orientation of water molecules, proteins can either remain in their native state, thus leading to a constructive interaction with cells, or can denature, with negative effects on cells [43]. A critical review on the major theories illustrating the foreign body reaction and the ways to control it for therapeutic purposes in contact with biomaterials was recently provided by Chandorkar et al. [44].

Since the surface features determine the type, amount and conformation of the proteins adsorbed, controlling the surface at nano-scale is a very interesting and valuable method to tune the cell-biomaterial interactions. There is a paucity of relevant studies in the field of bioactive glasses, but some interesting example can be found about bioceramics. Webster *et al.* [45] produced titania and alumina nanopatterned implants (32 and 23 nm grain-sized, respectively) and noticed that there was a significant increase in osteoblast adhesion in fetal bovine serum compared to smooth surfaces. Since the increase of cell adhesion was observed for both types of nanomaterials, it was hypothesized that the interaction between the proteins (and later the cells) and the implant surface is independent of the surface chemistry but mainly relies on the nano-topography [45].

### **3. BASIC ASPECTS ABOUT MANUFACTURING OF CERAMIC AND BIOACTIVE GLASS-DERIVED SCAFFOLDS**

#### **3.1. Overview of the fabrication strategies**

The first attempt to produce a bioactive glass-based scaffold was made in 2002 by Sepulveda *et al.* [46]. The manufacturing method was based on a sol-gel process combined with *in situ* foaming in order to obtain a macro-porous structure [46]. Since then, a lot of research groups had gone through a multitude of studies trying to find the optimal manufacturing process to

fabricate an “ideal” scaffold. This process should allow obtaining scaffolds with bone-like mechanical properties, controlled porosity, adequate surface topography and free from any toxic substances (e.g. solvents or additives needed for the production route). Furthermore, an ideal scaffold should be reliable and repeatable, in order to guarantee a mass production with constant features. On the other hand, customizability may be an important added value to meet the needs of each patient. Last but not least, the manufacturing of the scaffold has to be economically convenient, fast and as safe as possible regarding both the workers involved and the environment [47].

The technologies that have been developed so far for the production of bioactive ceramic and glass-based scaffolds can be categorized in two main groups, i.e. conventional methods and additive manufacturing techniques (also referred to as rapid prototyping (RP) or solid freeform fabrication (SFF)) [48]–[51]. The first group of methods follows the top-down manufacturing approach, which involves the removal of selected pieces/parts from a bulk material in order to create the wanted shape and porosity. They are also collectively called subtractive manufacturing technologies since the material that composes the scaffold is removed after the initial fabrication. The second group includes the technologies that involve a bottom-up approach, i.e. the scaffold is built according to a layer-wise approach (or “piece by piece”). A short overview of the above-mentioned techniques, which will be described in detail in the sections 4 and 5, is reported in **Table 2**.

It is important to notice that almost every method used for the production of ceramic and glass-based scaffolds – but the case of composites with polymers – involves a final consolidation step (high-temperature sintering). This is a crucial issue in the field of bioactive glasses since devitrification of the material during sintering (sinter-crystallization) usually leads to a decrease of the bioactive properties (apatite-forming ability).

In this regard, Filho et al. clearly showed the decrease of apatite formation in devitrified 45S5 Bioglass<sup>®</sup> when the crystallization exceeds 60% [52]. A similar behavior was also observed in the case of S53P4 glass (53SiO<sub>2</sub>-20CaO-23Na<sub>2</sub>O-4P<sub>2</sub>O<sub>5</sub> wt.%): the crystallization of the parent glass did not totally suppress the apatite formation on the sample surface but it decreased the formation rate and thickness of the reaction layer [53]. Massera et al. [54] reported that crystallization can even prevent the apatite layer formation *in vitro* for partially-crystallized phosphate glasses.

On the other hand, sintering at a too low temperature may produce incomplete or poor densification resulting in low mechanical properties. Therefore, the knowledge of the thermal behavior of the material is key for the appropriate selection of the sintering treatment.

### 3.2. Sintering of crystalline ceramics and glasses

Sintering is the consolidation process of a previously-shaped body, called “green body”, which may be formed out of ceramic (glass) powders only by means of pressure, or a mixture of powders and a binder, such as water or a polymeric oil. Sintering is a thermal process achieved by heating the green body at a temperature usually between 50 and 75% of the melting temperature and keeping it at this temperature for a certain period of time. In this way, powders densify, generating chemical bonds between them and reducing the green body volume (shrinkage) [55].

An external pressure may be optionally applied as an aid to the process (sintering under pressure); otherwise, the process is called pressureless (or conventional) sintering. Another classification is based on the different diffusion mechanisms that can occur during sintering:

- Solid state sintering: the only phase that is present during the process is the solid one, without formation of a liquid. The main mechanism for the densification is diffusion in the solid state.

- Accepted Article
- Liquid-phase sintering [56] implies that a liquid (5-10 vol.%) forms during the sintering cycle. Early uses of this method involved firing ceramics with a glass additive that, at high temperatures, turns into a viscous liquid. In the typical situation, the solid grains are soluble in the liquid. This solubility causes the liquid to wet the solid, providing a capillary force that pulls the grains together. At the same time, the high temperature softens the solid, further assisting densification. High-diffusion rates are associated with liquids, thus leading to fast sintering or need for lower sintering temperatures. A limitation of this strategy is the decrease of the maximum application temperature of the sintered material due to the relatively low softening point of the solidified liquid phase (compared to that of the major ceramic phase).
  - Vitrification: it occurs when the amount of liquid phase is high enough to fill the pores. This typically requires more than 25 vol.% of liquid that can be formed by a reaction between solid state precursors or by melting of one of them. During cooling, the liquid phase can either crystallize or vitrify.
  - Viscous sintering: this process involves the heating of a glass mass above or near its softening temperature and the densification of it by viscous flow under the effect of surface tension forces.

Furthermore, sintering can be reactive or non-reactive depending on if the precursor particles can chemically react one another forming new phases during the heating or not [55].

Removal of the binder prior to consolidation is recommended in order to avoid any contamination that could change the properties of the resulting sintered product.

### 3.2.1. Thermodynamic driving force: reduction of the free energy

The driving force of the sintering is the reduction of the total surface free energy of the compound. The total surface energy of the compact is expressed as  $\gamma A$ , where  $\gamma$  is the specific surface energy of the solid-gas interface and  $A$  is the total surface area. Thus, the reduction can be expressed according to **Equation 1**:

$$\Delta(\gamma A) = A\Delta\gamma + \gamma\Delta A \quad (1)$$

where  $\Delta\gamma$  is the variation in the surface energy due to the reduction of the solid-gas interface, which leads towards densification of the compact [57]. On the other hand, a reduction of the surface area,  $\Delta A$ , leads to coarsening without densification. The first path results in a correct sintering, whereas the second one leads only to a grain growth without the removal of the pores (**Figure 2**). Both paths that lead to a decrease in total surface energy may occur simultaneously, but usually, the surface area reduction happens at a lower temperature than the densification.

After the densification of the powders, a stage of grain growth may occur, which is called Ostwald ripening. This is due to the fact that grain boundaries are high-energy areas and, hence, they tend to be minimized to reduce the total energy. This thermodynamically-driven process occurs because large particles are more energetically stable than small particles (the internal pressure is reversely proportional to the radius of the particles). Large particles, with their lower surface-to-volume ratio, have a lower surface energy. As the system tries to lower its overall energy, the atoms on the surface of a small particle will tend to diffuse into the surface of larger particle. Therefore, all smaller particles shrink while larger particles grow, and overall the average particle size increases. This effect clearly appears in both solid-state and liquid-phase sintering. Since the densification rate lowers as the grain size increases, it is unlikely that the compact densifies after coarsening, unless pressure is applied to support densification [57].

### 3.2.2. Kinetic aspects: formation of sintering necks and diffusion

Referring to solid state sintering, it is possible to describe the sintering process by dividing it into different steps. The first one, the initial stage, involves the creation of necks between two different grains. This leads to a moderate shrinkage, about 5 vol.% if coarsening does not occur. During the intermediate stage, there is the diffusion of material from the grains to the void spaces in order to reduce the total surface energy. At the end of this stage, the compact has been turned into a 3D structure with a network of interconnected channel-like pores. This stage ends when only 5-10 vol.% of porosity is left. The final stage starts when the pore network starts to break into isolated closed pores and coarsening takes place more substantially – this is why it is hard to remove the last pores.

In order to describe the basic theory for sintering, the particles are approximated to a spherical shape. Since powders are not an infinite flat surface, the equilibrium pressure between the solid and the gas phases is different from the vapor pressure,  $P_{\infty}$ . According to the Laplace law (**Equation 2**), the internal pressure,  $P_i$ , for a sphere with radius  $r$  is:

$$P_i = P_{\infty} + \left(\frac{2\gamma}{r}\right) \quad (2)$$

where  $\gamma$  is the surface tension between the gas and the solid.

The same formula can be applied for a pore but the radius is considered negative. The inner pressure in a spherical grain is greater than the one on an infinitely flat surface. In the case of two grains connected by a neck, i.e. a toroidal shape with concave sides (**Figure 3**), the external surface is in compression and the neck surface is in traction. This results in the creation of a different pressure in the bulk that leads to a material flow from the grain to the neck region. For the same reason, there is also a difference in the vapor pressure between the grain surface and the neck area, also provoking a process of evaporation and condensation and a gas-phase diffusion [58].

Depending on the site from which the atoms are diffusing, there are different mechanisms of diffusion that lead to different results in terms of both densification and microstructure. Bulk, grain surface, and grain boundaries can be sources of material. Atoms can diffuse through different means, which also implies that different diffusion coefficients control the rate of their flows. During sintering, several kinds of diffusion can occur, e.g. on the surface, inside the grain lattice, between grain boundaries and on gas phase [58].

If the material source for diffusing atoms is the grain surface, there will be no appreciable densification as the distance between the centers of the grains does not change. On the other hand, if atoms come from the bulk or the grain boundaries, densification will occur as the centers of the grains will come closer. Depending on the mechanism, different parameters can control the process (**Table 3**).

Multiple mechanisms can occur at the same time with synergistic effects. The neck creation and growth rate primarily depend on the radius of the particles (the smaller the radius is, the faster the neck grows) and on the temperature (via an Arrhenius-type equation).

### *3.2.3. Microstructure*

The control of the final microstructure is essential to obtain a high-performance ceramic body. Given the brittle nature of ceramics and glasses, if a too large porosity remains in the sintered material, the mechanical properties will be greatly affected. This issue is particularly important considering that scaffolds should indeed be inherently porous, but the struts/walls of the solid skeleton have to be well-densified. In this regard, the difficult sintering of 45S5 Bioglass<sup>®</sup> led to the fabrication of dramatically brittle glass-ceramic foams with hollow struts (compressive strength <0.5 MPa) [59].

The movement of the grain boundaries can be limited by the presence of second-phase precipitates and pores. Pores can also move and their mobility depends on the pore size and the involved diffusion mechanism. Depending on the velocity of the pores with respect to that of the grain boundaries, different microstructures may occur:

- pores with the same velocity as the grain boundary: pores can travel and merge with other pores. The result is an inter-granular pore.
- pores much slower than the grain boundary: the pore and the grain boundary separate and the growth rate of the grain increase. The pore will be incorporated, and there can be several big grains with many intra-granular pores [58].

#### *3.2.4. Liquid-phase sintering*

The above-reported considerations mainly apply to solid state sintering, which is the easiest case to model and discuss. Different mechanisms are involved when a liquid phase appears during the sintering. This liquid might come from some of the components of the materials or be originated by introducing sintering aids (e.g. small amounts of glass having lower viscosity at the sintering temperature) in the green body.

In the presence of a liquid during the sintering, different phenomena take place:

- the adhesion between grains is increased;
- the migration of the liquid can close some of the pores and promote a certain shrinkage. Since the liquid fraction is low (typically <10 vol.%), it is not capable of eliminating all the pores by this mechanism;
- atomic diffusion in the liquid phase is speeded up.

In general, wetting the grain boundaries with a liquid is useful to reduce surface energy and, thus, the presence of a liquid allows a good densification to be easily achieved. The liquid formation is more controllable if it comes from a sintering aid rather than from an incongruent melting of one of the compounds. This liquid can either be permanent, being present throughout the sintering and solidifying at the end of the process, or disappear during the sintering.

The liquid-phase sintering can be divided into four different processes according to the theory developed by Cannon and Lenel and following evolutions [60]:

1. formation of the liquid phase (from melting or chemical reactions) in the compact of powders;
2. due to the formation of capillary stress, the particles of the green body are rearranged;
3. solution-precipitation processes lead to the densification of the material;
4. a further densification is achieved through the removal of the pores entrapped in the liquid phase.

During the initial stage (point 1), the wetting angle ( $\theta$ ) plays a crucial role in the flow of the liquid. If it is greater than  $90^\circ$ , the liquid does not wet the particles and there is no flow. If  $\theta$  is less than  $90^\circ$ , a liquid flow can start due to capillary forces. The pressure gradient causes the rapid flow of the liquid, the rearrangement of the solid particles and pores filling. Moreover, there is less pressure inside the liquid meniscus than in the pores, thus the capillary forces generated keep the grains together. The first stage is over when all the solid particles are coated by a thin liquid film and the fluid is dispersed homogeneously within the compact, reducing gas-solid interfaces [58].

During the intermediate stage (points 2 and 3), the grains partially dissolve in the liquid and the material diffuses towards the surface of the liquid, where precipitation takes place. The consequences of this process are a flattening of the contact area, a modification of the grain shape and a reduction of the porosity, which lead to the densification of the compact.

The final stage (point 4), which involves solid-solid state sintering, occurs when the contribution of the dissolution/precipitation process to the densification is negligible. In this stage, all the mechanisms of the solid-state sintering are active and lead to the final density of the ceramic body.

### *3.2.5. Sintering of an amorphous material*

Since amorphous materials do not have a crystalline structure and, therefore, grains that can coarsen do not exist, the predominant sintering mechanism for glasses is the viscous flow process. In this case, the fundamental parameters involved in the sintering are the heating rate and the viscosity of the material, as a function of the temperature. The latter parameter influences the models that can be used to represent the kinetics of the sintering process, and the former one can change the densification curve of the glass. In fact, the higher the heating rate, the higher the temperature to obtain a certain densification in the same time frame (there is a time lag).

In order to obtain high-density glasses, the sintering temperature should be lower than the onset of crystallization [61], [62]. If crystals form inside the material upon sintering (sinter-crystallization), the viscous flow will be less efficient or will completely stop, thereby resulting in poorly sintered glass-ceramic products. This is what happens during sintering of 45S5 Bioglass<sup>®</sup>, where crystallization is concurrent to densification [63].

## 4. SCAFFOLD MANUFACTURING BY “CONVENTIONAL” TECHNOLOGIES

The “conventional” technologies include all the manufacturing methods except for the ones that involve the replication of a virtual model by a CAD/CAM strategy (additive manufacturing). All these methods, generally, allow producing glass, glass-ceramic and polymer/glass composite scaffolds. Each approach is detailed into the next sections.

### 4.1. Foaming methods

These methods involve the use of a foaming agent and melt-derived or sol-gel bioactive glasses. Usually a slurry or a colloidal suspension (sol) is prepared and the foaming agent is added to create air bubbles that generate the porosity. Methods for producing the pores in the scaffold include direct injection of gases, vigorous agitation, gas generation through a chemical reaction, or thermal decomposition of peroxides [64].

Typical drawbacks of the foaming techniques are the presence of closed pores, low interconnectivity of the porous network, the formation of a non-porous outer layer and mechanical properties just acceptable (high brittleness of the scaffolds). Details of specific methods can be found in next sections.

#### 4.1.1. Gel-cast foaming

Gel-casting is a complex-shape process that uses melt-derived glass powders mixed into a solution of organic monomers, forming a slurry. The slurry is then poured into a mold, and then the polymerization initiator and catalyst are added. The polymerization takes place *in situ*, inside the mold; the polymeric gel allows the desired shape to be maintained. After the extraction from the mold, it is necessary to remove the solvent and the polymeric phase. If the

solvent used is water, it can be removed by simply drying; then, the green body undergoes pyrolysis in order to burn out the organic components and final sintering. In the early age of the gel-casting process, it was developed by using multifunctional acrylate monomers in organic solvents, but the use of non-aqueous solvents involved environmental problems and high costs. Therefore, efforts were made to use water as a solvent for acrylamide gel systems [65].

In order to use this manufacturing method to obtain porous scaffold for bone regeneration, it is fundamental to introduce a foaming step during the gelation process. The foam can be produced either by injection of gases or by mechanical frothing, but in most of the cases a surfactant is required to be added to the powder solution to stabilize the air bubbles. A key parameter to tailor scaffold porosity is the so-called *induction period* or *idle time*, which is the time that occurs between the addition of the initiator and the catalyst to the suspension and the beginning of the polymerization/ setting of the final structure. During the induction period, it is possible to mold the foam in the desired shape and changes in the bubble structure may take place. Two opposed processes come about, i.e. a thinning process of the lamellae that surround the bubbles and a thinning-resistant mechanism. The former causes local depression and is associated with drainage due to gravity or capillary forces/Van der Waals attractions that occur between thin films. The latter is associated with the high viscosity of the liquid, surfactant chain cohesion, elasticity of the surfactant walls and electrostatic repulsion between the two sides of a very thin film. All these mechanisms can result in the shrinkage and disappearance of some bubbles and in the coalescence of some other ones. A fine control of the chemistry and kinetics of these processes is necessary to obtain a suitable structure for bone-like scaffolds exhibiting, for example, open porosity and well-densified walls [66].

On this matter, Wu *et al.* [67] produced gel-cast bioactive glass foams using ICIE-16 melt-derived glass (49.46% SiO<sub>2</sub>, 36.27% CaO, 6.6% Na<sub>2</sub>O, 1.07% P<sub>2</sub>O<sub>5</sub>, 6.6% K<sub>2</sub>O, mol.%). By careful optimization of the major processing parameters, such as particle size, type of catalyst, surfactant, monomer and sintering treatment, scaffolds with a modal pore size of 379 μm and modal interconnect size of 141 μm were achieved (**Figure 4-a**), which are suitable for bone regeneration. The compressive strength was close to the lower limit of the trabecular bone (1.9 MPa) and HA was found to form after 3 days of immersion in SBF [67].

#### 4.1.2. Sol-gel foaming

The fabrication of porous scaffolds made from sol-gel glasses was first reported by Sepulveda *et al.* in 2002 [46]. The use of sol-gel glasses to produce amorphous scaffolds was due to the lack, at that time, of melt-derived bioactive glasses that could undergo a sintering process without crystallizing. The introduction of a foaming step during the sol-gel synthesis of the glass was necessary to obtain a porous structure. Unlike the gel-casting foaming, where the glass has been previously prepared, sol-gel foaming involves the formation of the macro-porous structure simultaneously to the glass synthesis. Since the gelation time for conventional sol-gel materials is a few days, it is also necessary to add an accelerator along with the surfactant. For example, Sepulveda *et al.* [46] used hydrofluoric acid (HF) to decrease the gelation time; the surfactant (polyethylene glycol) and the catalyst were added after the completion of the hydrolysis of the alkoxide precursors, under vigorous agitation. When the right viscosity was reached, the gel was poured into a mold and left to age. Afterwards, the evaporation of the solvent was carried out and the structure was sintered. A double-level porosity is achievable by this process. i.e. an interconnected macro-porosity (**Figure 4-b**) due to the surfactant action (air bubbles) and a nano-porous structure (mesopores within 10-30 nm) due to the intrinsic sol-gel texture [46]. The major drawback of sol-

gel materials is the high brittleness; however, recent optimization of the process allowed obtaining hierarchical scaffolds with a compressive strength of 5 MPa, which is in the range recommended for cancellous bone repair [68].

The dimensions of sol-gel glass scaffolds can be larger than those of sol-gel monoliths (up to several centimeters). Furthermore, crack formation is typically avoided due to the thin walls of the foamed structure, which reduce the path for the evaporation of water through the nanopores. The final porous structure can be designed, to some extent, by a careful tailoring of the process parameters such as glass composition, type of surfactant, catalyst and temperature [69].

While most of sol-gel bioactive glass foams are based on relatively simple binary ( $\text{SiO}_2\text{-CaO}$ ) or ternary compositions ( $\text{SiO}_2\text{-CaO-P}_2\text{O}_5$ ) [70], [71], some researchers have also incorporated additional modifiers in the wet synthesis to impart extra-functionalities, such as antibacterial properties (due to the release of  $\text{Ag}^+$  ions) [72] and magnetic properties (due to the presence of Fe ions and Fe-based magnetic phases) [73].

It is also possible to obtain sol-gel glass-based scaffolds by *in situ* foaming. Rainer *et al.* [74] produced a scaffold mixing silicate sol-gel glass with diisocyanate and a polyol, which are precursors of polyurethane (PU). The polymerization was conducted in the presence of a catalyst and a surfactant, and water was used as a foaming agent (it reacts with isocyanate groups producing carbon dioxide). As a result, a glass-loaded PU foam was obtained that eventually underwent thermal treatment (PU burning-out and glass sintering). The final scaffold exhibited a total porosity of 48 vol.% with a median pore diameter of 50  $\mu\text{m}$ , but it had also pore larger than 200  $\mu\text{m}$  (**Figure 4-c**) [74].

### 4.1.3. $H_2O_2$ foaming

Another approach to obtain porous structures by means of a foaming agent is based on the use of peroxide solution. If the peroxide solution is heated at around 60 °C, it will release water vapor and oxygen that can be used as foaming agents to produce bubbles and, hence, macro-pores in the scaffold. Navarro *et al.* [75] mixed phosphate glass powders (molar composition: 44.5%  $P_2O_5$ , 44.5% CaO, 6%  $Na_2O$ , 5%  $TiO_2$ ), sieved below 30  $\mu m$ , with different amounts of  $H_2O_2$  solution; the slurry was then cast into a mold, foamed for 2.5 h at 60°C, dried and sintered. The influence of the amount of  $H_2O_2$  solution, as well as the time and temperature of thermal treatment, on the scaffold architecture was studied. Specifically, it was observed that the main factor affecting the macroporosity of the scaffolds was the  $H_2O_2$  percentage included in the mixture. Although the  $H_2O_2$  decomposition process led to an aleatory distribution of the pores and interconnectivity level, an increment in the porosity, pore size and interconnectivity degree was observed as the  $H_2O_2$  content increased (maximum total porosity 55 vol%, pore sizes ranging from 20  $\mu m$  to 500  $\mu m$  [75] (**Figure 4-d**)).

### 4.2. Thermal consolidation of particles

All these methods involve the mixing/incorporation of sacrificial particles/template in the green body that usually undergoes sintering. Pore-forming agents are typically polymers of natural (e.g. starch, rice husk) or synthetic origin (e.g. polyethylene (PE) particles). These techniques are relatively low cost and allow obtaining easily bioceramic and glass products of complex shape, thanks to the advanced forming technologies of the green bodies. The level of porosity can be tailored by controlling the advancement of densification and, moreover, a structure with gradients of porosity can be fabricated by combining sacrificial

templates/particles with different characteristics. On the other hand, it is generally difficult to obtain high levels of porosity (>70 vol.%) and good pore interconnectivity [64].

#### 4.2.1. Scaffold manufacturing without the use of porogen particles

In this kind of process, no sacrificial phases are added to the ceramic or glass particles used to create the green body. The porosity is controlled only by varying the size of the particles and the sintering process. In fact, in order to obtain a porous scaffold at the end of the process, the sintering has to be stopped as soon as sintering necks are formed between the particles and they are enough to confer adequate mechanical properties to the final porous product. This technique is very simple and does not require controlling the dispersion of porogen particles throughout the volume of the green body. On the other hand, it allows obtaining only low-porosity scaffolds (typically below 50 vol.%) and a strict control of the particle shapes and sizes are necessary since these parameters affect strongly the final properties of the scaffold.

Fu *et al.* obtained a scaffold shaped in the form of the articulating surface of a proximal tibia by using 13-93 glass (53SiO<sub>2</sub>-6Na<sub>2</sub>O-12K<sub>2</sub>O-5MgO-20CaO-4P<sub>2</sub>O<sub>5</sub> wt.%) (**Figure 5**) [76].

The glass particles were sieved in the size range of 255 to 325 μm. Slip-casting was used as a forming method employing an aqueous solution of poly (vinyl alcohol) as a binder. As a result, an amorphous scaffold with 40 vol.% of porosity and pore interconnections within 100-300 μm was obtained. The compressive strength (22 MPa) was low compared to that of the cortical bone but suitable for replacing cancellous bone. Indeed, higher compressive strength is achievable by reducing the porosity and increasing the densification [76].

Borate glass-based scaffolds have also been obtained by Liang *et al.* through the same technique [77]. Scaffolds were manufactured by using spheroidal or irregular particles with nominal dimensions within 90-425 μm; a maximum porosity of 40 vol.% was achieved with bigger and irregular particles due to the less efficient packaging and sintering process

compared to the spherical and smaller ones, respectively. Neither pore characteristics (e.g. size and interconnections) nor mechanical properties were reported, but the scaffold morphology was similar to that obtained by Fu *et al.* [76].

Polymer/glass composite scaffolds were also obtained by this method. Lu *et al.* used microspheres made of poly(lactic-co-glycolic acid) and 45S5 Bioglass<sup>®</sup> to obtain a porous structure with total porosity around 40 vol.% and compressive strength close to the lowest threshold of the cancellous bone [78].

#### 4.2.2. Polymeric fillers used as porogen particles

In order to increase the porosity of the scaffolds and have a better control on the shape and dimension of the pores, a polymeric filler can be mixed with the inorganic particles before molding. These sacrificial particles should be fully removed prior to the sintering process so that no residual contamination is left in the sintered scaffold. In fact, if the removal step is not well controlled, black char (organic combustion residue) may form on the surface of the green body, thus precluding good sintering and decreasing the bioactivity of the glass.

##### 4.2.2.1. Synthetic polymeric fillers as porogens

Relatively inexpensive synthetic polymeric particles have been mixed to glass powders and used as thermally-removable pore forming agents for producing scaffolds. In 2001, Livingston *et al.* [79] obtained a porous scaffold using 45S5 Bioglass<sup>®</sup> particles mixed with camphor (C<sub>10</sub>H<sub>16</sub>O) (**Figure 6-a**). They mixed glass powder (38-75 μm) with sacrificial particles having a size within 210-350 μm; then the green compact, obtained by dry pressing, underwent a heat treatment at 640°C for 30 min in order to remove the camphor

and sinter the glass particles. The resulting scaffolds presented a 40% crystallization degree, 21 vol.% of porosity and pore size in a range of 200-300  $\mu\text{m}$  [79].

PE powders in different size ranges (100-300  $\mu\text{m}$  and 300-600  $\mu\text{m}$ ) were used by Vitale-Brovarone *et al.* as organic filler [80] (**Figure 6-b**). Different porous scaffolds have been prepared by mixing different volume fractions of PE particles (25-70 vol.%) and melt-derived glass sieved below 106  $\mu\text{m}$ . Changing the amount and size of PE particles, macro-pores within 100-200  $\mu\text{m}$  or above 200  $\mu\text{m}$  were obtained, with a total porosity from 50% to 70% and good interconnectivity between the pores. A maximum compressive strength of 6 MPa, comparable to that of trabecular bone, was obtained for small amounts and sizes of PE particles. Micro-pores below 10  $\mu\text{m}$ , associated with the presence of  $\beta$ -wollastonite crystals on the surface of the pore walls/struts, were also reported [80].

More recently, paraffin wax was used as a pore-forming agent by Zhang *et al.* [81] to create scaffolds based on apatite/wollastonite glass-ceramics. Powders of paraffin wax (250-650  $\mu\text{m}$ ) were mixed with glass-ceramic particles (weight composition: 44.7% CaO, 16.3%  $\text{P}_2\text{O}_5$ , 34.0%  $\text{SiO}_2$ , 4.6% MgO, 0.5%  $\text{CaF}_2$ ) in different ratios; then, the compact was sintered at 1100  $^\circ\text{C}$  for 6 h to obtain a glass-ceramic scaffold. In this way, an interconnected porosity of 70 vol.% was obtained with macro-pores deriving from the thermal decomposition of the polymeric filler in the range of 250 to 350  $\mu\text{m}$ . Mechanical properties showed a strong dependence upon the total porosity, but the minimum value was assessed at about 5 MPa, which is still acceptable for implantation in non-load-bearing bone sites. The apatite-forming ability of these glass-ceramic scaffolds was proved by immersion tests in SBF as well as the good biological compatibility with mesenchymal stem cells (MSCs) *in vitro* [81].

#### 4.2.2.2. Starch consolidation method

Sacrificial fillers of natural origin have also been used to obtain porous structures, such as starches of different plants (corn, rice and potatoes) that generate a gelled system with the glass powders and act as porogen particles during the thermal treatment, when they are burned-out leaving void spaces and pores. This technique was developed by Lyckfeldt *et al.* [82] in 1998, initially for alumina porous scaffolds.

The consolidation process is possible due to the ability of starches to absorb water when heated. Starch grains are insoluble in water below 50 °C, so it is easy to mix them with dry glass particles and handling them. During the water absorption around 70-80 °C, the starch particles swell irreversibly and lead to the gelation of the system associated with a great increase of the viscosity. Since starches remove water from the suspension by swelling, ceramic particles are forced to stack together thus increasing the strength of the green body.

Moreover, starch particles can inherently act as binders [82]. Some of the great advantages of this method include the very low cost of the starches and the non-toxicity of the reactants.

Different research groups used the starch consolidation method to manufacture bioactive glass scaffolds. As an illustration, Vitale-Brovarone *et al.* [83] tested the suitability of different kinds of starches, thus varying the structural and mechanical properties of porous scaffolds based on a 50SiO<sub>2</sub>-25CaO-16Na<sub>2</sub>O-9MgO (mol.%) glass system. They prepared different samples using corn, rice and potato starches by mixing the organic particles (sieved below 63 μm) with glass powder (sieved below 106 μm) under magnetic stirring and heating up to 80 °C. When the gelation point was reached, the solution was poured into a mold and the residual water was removed. A two-step heat treatment was necessary for the burning-out of the organic phases and the sintering of the glass, respectively. Initial trials revealed that the organic content had to be in the range of 20 to 26 wt.% for achieving a compromise between adequate porosity, pore size and effective densification of the solid fraction. Corn starch

grains, having too low dimensions, resulted in a too small pore size compared to cancellous bone and, therefore, their use was considered a non-optimal choice. In general, this method allows obtaining scaffolds with interconnected pores in the dimensional range of 50 to 100  $\mu\text{m}$  (**Figure 6-c**) and compressive strength (6 MPa) comparable to that of cancellous bone [83], [84].

#### 4.2.2.3. Rice husk method

In the last decades, there were huge efforts to reduce waste generation in many industrial processes or, at least, to find another way to reuse and recycle waste products. One example of a waste material with high availability is rice husk, especially in those countries that produce it [85]. Rice husk is obtained during the refinement of rice, after the harvesting. It is a valuable material that contains mostly organic substances ( $\approx 75$  wt.%) but also amorphous silica ( $\approx 15$  wt.%) and water [85]. For example, rice husk is used during the synthesis of silicon carbide whiskers that act as a strengthening phase in ceramic- and metal-matrix composites.

In order to confer more value to this kind of waste, rice husk was also interestingly used as a porogen agent for the fabrication of 45S5 Bioglass<sup>®</sup>-based scaffolds by Wu *et al.* [86] They used the original 45S5 glass sieved into two different size ranges, i.e. below 25  $\mu\text{m}$  and within 25-75  $\mu\text{m}$ , and studied the effects of different amounts of rice husk on the porosity and mechanical strength of the final sintered scaffolds. Samples were fabricated by mixing of 45S5 glass powders and rice husk grains with different dimensions (below 355  $\mu\text{m}$  and within 355-600  $\mu\text{m}$ ) and in different weight ratios; a poly (vinyl alcohol) (PVA) aqueous solution was used as a binder. After uniaxial pressing, the green compacts underwent a burning-out stage at 450 °C followed by sintering at 1050 °C to obtain partially crystallized scaffolds. Morphological analysis showed the presence of elongated pores with different sizes

(Figure 6-d), which was due to the typical shape of the rice husk. Pore size ranged from 25 to above 420  $\mu\text{m}$ , but the smaller ones were usually isolated and poorly interconnected. Similarly to the porous bodies produced via other techniques of organic filler burning-out, these scaffolds also exhibited a lower porosity (43-49 vol.%) than that of cancellous bone, while the compressive strength (5-7 MPa) was suitable for osseous repair [86].

#### 4.2.3. Porous polymer replication

In order to achieve a higher level of porosity and a more bone-like structure exhibiting interconnected macro-pores, researchers started to use polymeric foams as templates for producing biomedical scaffolds. The ability to obtain polymeric foams with a very controlled 3D pore/strut architecture has been well demonstrated, and structures with fully-open porosity and more than 90 vol.% of voids are easily achievable. The basic idea was to replicate the foam structure by coating the struts and walls using a glass (ceramic) slurry and then to consolidate it. Composite, glass and glass-ceramic scaffolds can be obtained depending on whether or not a burning-out treatment is carried on.

##### 4.2.3.1. Coating method

This approach allows polymer/glass composite scaffolds to be produced. Different kinds of polymeric substrates, including foams, meshes and fibrous bodies, can be coated using different methods, such as electrophoretic deposition (EPD) and slurry dipping. In these techniques, neither sintering stages nor burning-out treatments are carried out, in order to maintain the organic phase stable in the final product. Composite scaffolds typically exhibit a polymeric core and a bioactive glass surface coating. The polymeric core increases the toughness of the scaffolds and tunable absorbability can be achieved depending on the polymer used [78].

One example of such scaffolds can be found in the work of Roether *et al.* [87] who coated poly(DL-lactide) biodegradable polymeric foams, obtained through induced phase separation followed by freeze-drying, by means of slurry dipping technique and EPD using a slurry made of 42 wt.% of 45S5 glass in water. EPD-assisted coating method was possible due to the presence of charged particles in the suspension. The polymeric foam showed a highly oriented porous structure of tubular macro-pores (>100  $\mu\text{m}$  in diameter) interconnected with small pores within 20-30  $\mu\text{m}$ . Slurry dipping proved to offer more control on the coating thickness and a better replication of the foam (**Figure 7-a**), while EPD was prone to occlude some of the pores [87].

It is worth noting that EPD has also been successfully used to deposit a layer of bioactive glass on the struts of mechanically-strong but almost-inert ceramic scaffolds [88]. In this way, multifunctional properties can be imparted to the porous substrate, namely apatite-forming ability [89] and controlled release of therapeutic agents (e.g. strontium ions that can reduce bone resorption in osteoporotic patients) [90]. Bioactive glass coatings on porous silicate glass-ceramics were also produced by simple dipping in a sol or glass slurry, but this approach provided less control on the coating characteristics (e.g. thickness, homogeneity, reproducibility) compared to EPD [91].

Following the same rationale, Yu *et al.* [92] recently deposited a sol-gel bioactive glass coating onto wood-derived carbon scaffolds (**Figure 7-b**). The hierarchical bimodal pore structure (pore size around 50 and 5  $\mu\text{m}$ , respectively) derived from beech wood was retained in the glass-coated scaffolds after thermal stabilization of the glass in argon to avoid the burn-off of the carbonized skeleton. The glass layer imparted bioactive properties to the otherwise bioinert carbon skeleton, as confirmed by the formation of nanocrystalline HA on the pore walls of the samples *in vitro*.

Lao et al. [93] coated gelatin scaffolds with a bioactive glass layer by a simple dipping process in the sol without performing a high-temperature treatment. This was possible due to the use of calcium ethoxide as CaO precursor: while other calcium sources, such as calcium salts, require thermal stabilization above 400 °C to make calcium ions enter the silicate network, calcium alkoxides can be incorporated into the silicate network at room temperature as a result of the hydrolysis and condensation reactions.

#### 4.2.3.2. Polymer foam replication

Contrary to the previously-described coating method, in the polymer foam replication the organic phase (sponge) is fully removed and it only aims to act as a template for the inorganic phase during sintering. Thus, after the coating of the foam with a slurry, the composite structure is subjected to a double-stage thermal treatment as to achieve the complete burning-out of the polymeric foam and to densify the ceramic/glass phase. Silicate, borate/borosilicate, and phosphate glass-derived scaffolds have been obtained by this method [94]. The foam replication has several advantages, such as the achievements of high-porosity levels (up to 90 vol.%) in trabecular structures that are very close to the cancellous bone. On the other hand, the scaffolds fabricated by sponge replication often may have inadequate mechanical properties for being implanted in bone [16].

The first use of this technique in the field of bone tissue engineering was made by Chen *et al.* in 2006 [95]. They used a PU foam as a sacrificial template, covered by a slurry containing 45S5 Bioglass<sup>®</sup> commercial powders and PVA as a binder. The coating was obtained by immersion of the foam in the slurry and following removal of the excess slurry by squeezing. The coating thickness is adjustable by multiple immersions. Then, the PU was removed by heat treatment and the glass is sintered. The porosity obtained in this way was very high (more than 90 vol.%) with a network of open and interconnected macro-pores in the range of

510 to 720  $\mu\text{m}$ . The structure is very similar to that of the cancellous bone, but the high level of porosity and the typical hollow structure of the glass-ceramic trabeculae due to inadequate sintering strongly affect the mechanical properties (**Figure 7 c-d**): in fact, the compressive strength of these 45S5-derived scaffolds was in the range of 0.1 to 0.4 MPa [95], which is below the typical threshold recommended for bone tissue engineering scaffolds (around 1-2 MPa [16]). Poor sinterability of 45S5 Bioglass<sup>®</sup> pushed scientists to develop glass compositions with a larger sintering window allowing the fabrication of mechanically stronger scaffolds. Fu *et al.* prepared foam-replicated 13-93 glass scaffolds having a compressive strength of 18 MPa [96]; even higher values (around 20 MPa) were obtained by processing a silico-aluminate composition [97], although the presence of  $\text{Al}_2\text{O}_3$  almost suppressed the apatite-forming ability of the material [98].

The polymer foam replication was also used to obtain 3D functionally-graded porous structures. Bretcanu *et al.* [99] fabricated 45S5-derived scaffolds with gradients of porosity just by pre-forming the PU foam before the infiltration with the slurry. In this way, they were able to produce continuous and stepwise structures mimicking more closely the architecture of cancellous bone. The foams were pre-formed by forcing them into 2D and 3D aluminum molds, and the change in the porous structure is directly related to the grade of compression of the foam in the mold. Then, the pre-formed foams were infiltrated as usual with a 45S5 Bioglass<sup>®</sup> slurry, the PU was burnt-out and the inorganic phase sintered [99]. **Figure 8** shows a scaffold obtained by pre-forming of a PU foam.

Polymer foam replication was also used to fabricate 1-mm thick curved scaffolds attached as trabecular coatings to the outer surface of ceramic acetabular cups [100]. In this innovative approach, instead of acting as a bone defect filler, the macro-porous scaffold was intended as the key component of a hip joint prosthesis able to promote implant fixation to bone via the bioactivity mechanism of bioactive glasses.

#### 4.2.4. Freeze-drying

Instead of using an organic template as a porogen agent, it is possible to take advantage of the formation of ice crystals to generate the porous structure of the scaffold. This approach was pioneered by Fukasawa *et al.* for the production of porous industrial ceramics via an environment-friendly method [101], [102], and was then optimized by Tomsia and co-workers in the attempt of developing super-tough nacre-like biomedical composites [103], [104]. The starting suspension of ceramic (glass) particles is subjected to a fast and directional freezing, resulting in the formation of elongated ice crystals of the solvent(s). Once the solvent has been removed, it is possible to consolidate the scaffold. The flexibility of this method is great and highly appealing as porous scaffolds can be obtained by using polymers, ceramics, and glasses (produced via both melting and sol-gel method).

##### 4.2.4.1. Freeze-casting of suspensions

In this approach, a colloidal suspension of glass particles is poured into a mold and then it is rapidly frozen. Since the cooling rate, usually, is not homogeneous in all directions, this leads to the formation of oriented and elongated ice crystals. The frozen solvent is removed by sublimation under vacuum at mildly “cold” temperature (around  $-20\text{ }^{\circ}\text{C}$ ). This step is crucial since an uncontrolled removal of the solvent can destroy the porous structure of the scaffold. Once the solvent is completely removed, the scaffold is thermally treated in order to sinter the inorganic particles. The main advantage of the freeze-casting is in the oriented microstructure of the pores, that confers to the scaffolds much higher compressive strength compared to the other method discussed in the previous sections. On the other hand, obtaining scaffolds with suitable pore dimensions for bone tissue engineering applications by only using water as a solvent is not possible, since the range of pore sizes that is achievable for such suspension is 10-40  $\mu\text{m}$ , which is too low compared to cancellous bone (well above 100  $\mu\text{m}$ ). In order to

obtain a larger pore size is necessary to include additional organic solvents in the solution, such as 1,4-dioxane, or to completely change the solvent, for example, camphene [16].

Fu *et al.* [105] manufactured a glass scaffold by using an aqueous solution of 60 wt.% dioxane as a solvent. They mixed 5-20% of very fine particles ( $<5\ \mu\text{m}$ ) of 13-93 glass with a disperser and 1% of PVA as a binder. After the directional freezing, performed using a cold steel plate, and the removal of the solvent, burn-out and a sintering steps were performed. The resulting microstructure showed ordinate columnar pores with diameters between 90 and 110  $\mu\text{m}$ . Varying the concentration of the glass particles affected the total porosity and the size of the single pores. The compressive strength of these scaffolds was about one order of magnitude higher than that of cancellous bone, ranging from 50 to 10 MPa as the porosity increases from 35 to 70 vol.% [105]. The same research group reported similar results by freezing camphene-based solutions [106]. Given the high mechanical properties and the columnar microstructure which reproduces, to some extent, that of cortical bone, these scaffolds show promise for the repair of load-bearing strong bones.

#### 4.2.4.2. Ice-segregation-induced self-assembly (ISISA) combined with the sol-gel method

Similar to the freeze-casting method, the ISISA of a sol involves the rapid freezing of a sol by immersion in liquid nitrogen at a controlled rate and then the sublimation of the frozen solvent. Tailoring the physico-chemical parameters of the process makes possible to achieve a sophisticated control on the resulting (oriented) microstructure. These parameters include the solvent composition, the concentration and nature of the solute, the temperature gradient and the cooling rate. Modifying the chemical composition of the sol allows achieving a great control over the size of the pores; furthermore, scaffolds with a pore-graded structure can be fabricated by changing the immersion rate.

Minaberry and Jobbagy [107] demonstrated the feasibility of this process by making a porous scaffold using a bioactive sol-gel-derived glass belonging to the SiO<sub>2</sub>-CaO system. After the gelation of the sol, the gel was poured into a mold and then dipped at defined rates into liquid nitrogen at -196°C. After the solvent removal, the green body was subjected to annealing in order to completely eliminate process residuals, such as salts, acid, organic molecules, and achieve a certain degree of consolidation. The cooling rate was shown to affect the oriented porous structure: in fact, higher rates favor super-cooling and the formation of a high density of small ice crystals, preventing the formation of large pores. Nevertheless, pores no larger than 20 µm were obtained and, due to the very thin walls and struts, low compressive strength was assessed (less than 0.2 MPa) [107]. Therefore, these scaffolds appear not very suitable for applications in clinics as they are brittle and have significantly smaller pores compared to trabecular bone.

#### 4.2.5. Thermally induced phase separation (TIPS)

This technique is mainly used to obtain polymeric scaffolds, but resorbable polymer/glass composites can also be produced. The process is based on the change of the solubility between two different polymers as a function of the temperature. In fact, two polymers can be totally soluble one into the other at a certain temperature but be almost totally insoluble at a lower temperature. If a solution of these polymers is prepared and then cooled under the upper critical solution temperature, they will separate, forming two distinguishable phases. With an adequate chemistry of the polymers is possible to control the amount of the two phases and their morphologies. One of the two phases will be rich in the polymer, while the other will be polymer-poor. The latter phase is the one that will be removed in order to obtain the porous structure. This technique allows highly porous structures to be obtained (up to 97

vol.% of porosity). Tissue engineering scaffolds can be made by TIPS that also incorporate glass nanoparticles for enhanced bioactivity [48], [78].

Maquet *et al.* [108] developed a composite scaffold based on 45S5 Bioglass<sup>®</sup> and bioresorbable polymers, i.e. poly(D,L-lactide) (PDLLA) and poly(lactide-*co*-glycolide) (PLGA). They made two series of samples, one for each polymer, varying the amount of glass powders (mean particle size around 5  $\mu\text{m}$ ). The suspension was obtained by mixing the polymer and the glass powder with a solvent (in this case dimethyl carbonate). The TIPS was achieved by immersion for 2 h in liquid nitrogen, and then the solvent was removed by freeze-drying under vacuum. Regardless of the glass-to-polymer volume ratio (10, 25 and 50 vol.%) and despite the mid-to-high solid content of glass particles, the porosity obtained was always very high (>90 vol.%). The effects of the different amounts of glass were a (moderate) decrease in the porosity and an increase in the apparent density whenever the glass-to-polymer ratio increased, a change in the shape of the pores and the dispersion of the particles, which was more uniform with higher amount of glass. At lower content, 45S5 Bioglass<sup>®</sup> particles did not interfere with the crystallization of the solvent, thus the pore morphology was similar to that of the pure polymer foam, in which a preferential orientation of pores was observed. On the contrary, at higher glass content, the pore shapes were more irregular. The addition of 50 vol.% of glass in the composite allowed doubling the elastic modulus of PDLLA- and PLGA-based composite scaffolds (around 25 MPa) compared to the neat polymer foams [108]. However, this value still remains far from the typical range of cancellous bone (50-500 MPa [109]).

#### 4.2.6. Solvent-casting and particulate leaching (SCPL)

Just like TIPS, also this process allows fully-polymeric and polymer/glass composite scaffolds to be fabricated. The concept behind this method is the solvent-casting technique,

where a polymer solution is poured into a mold and consolidated removing the solvent by means of evaporation or lyophilization, thereby obtaining a nano-porous structure. In order to obtain macro-pores, a water-soluble salt must be added to the solution as porogen particles. After the removal of the solvent, the structure is immersed in water and the salt particles are leached away so that pores are formed. All the required steps are summarized in **Figure 9**. This technique allows obtaining scaffolds with high porosity level (greater than 90 vol.%) and macro-pores having dimension up to 500  $\mu\text{m}$ , as well as a good control on the size and shape of the pores. Changing porogen morphology, dimension and total amount has a direct impact on pore characteristics and allows a certain control on them. Moreover, this technique does not require any advanced and expensive equipment. Nevertheless, several drawbacks have to be taken into account: final shapes of scaffolds are limited to flat sheet and tubes; retention of toxic solvents is possible; in case of biological molecules and proteins incorporated in the scaffolds, they can be denatured by the solvent, decreasing their activity; shapes of porogen are limited (water-soluble salt particles are usually cubic-like, spherical or equi-axed); a good interconnected pore network is difficult to achieve. Polymer/glass (ceramic) composites can be achieved by mixing the desired particles within the solution. Thus, for example, polymer-matrix scaffolds embedding hydroxyapatite or bioactive glass inclusions were obtained [78], [110].

Recently, Niu *et al.* [111] produced a scaffold via SCPL with a hierarchical structure, incorporating particles of mesoporous silica-based bioactive glass (m-BG) derived from the sol-gel process. The particles synthesized by this method show a highly-ordered structure of nano-sized channels with an average dimension of 5 nm. The m-BG powders were mixed with poly(L-lactide) (PLLA) in different weight ratios (15/30%) and NaCl particles (size around 400  $\mu\text{m}$ ) were used as a leaching porogen. After removing the solvent and leaching away the salt, the authors of this study assessed that the different amount of m-BG did not

affect the porosity obtained, which was around 70 vol.% in both cases, but had a huge effect on the morphology of the surface. With the lower glass-to-polymer volume ratio, the surface was smoother and more similar to the pure polymer scaffold, while the higher ratio was associated to a coarse surface. The presence of the glass also increased the compressive strength of the scaffold, reaching the mean value of 4.2 MPa [111].

## **5. SCAFFOLD FABRICATION BY ADDITIVE MANUFACTURING**

In recent years, a whole new kind of manufacturing technologies has come out: the additive manufacturing technologies (AMTs). The first one was developed in 1986 by Chuck Hull and it was based on stereolithography [112]. The AMTs, also known as rapid prototyping (RP) or solid freeform fabrication (SFF) methods, revolutionized the concept of fabrication in a lot of industrial sectors. They allow precisely controlling the construction of an object “layer by layer” or “piece by piece”, offering the opportunity to create shapes and details that cannot be achieved by conventional technologies. In addition, the level of flexibility, industrial scalability and customization provided by AMTs is enormous.

The starting point in all AMTs is a computer-aided design (CAD) model or even a computed tomography (CT) of the object that is intended to be reproduced. Then, it is slashed into layers along one of its axes and the AMT builds the object making each layer, one by one, according to a layer-wise strategy. Ideally, all kinds of materials can be processed by AMTs, ranging from metals to polymers, ceramics, glasses and even living matters (cells).

AMTs related to ceramic materials (and glasses) can be divided into two groups: direct and indirect fabrication techniques. By using direct AMT, it is possible to obtain a complete artifact without the need for a post-process treatment. In fact, direct AMTs melt (on the surface) and consolidate the ceramic particles during the shaping of the object, either by

means of a laser beam, in the case of selective laser sintering (SLS), or by electron beam melting (EBM). If post-treatments are needed, such as de-binding and sintering, the AMTs are referred to as indirect methods. Four categories of indirect AMTs exist, based upon the basic techniques:

- Laminated object manufacturing (LOM): the binders are included in the feedstock and sheets of materials are glued together and then cut in the suitable shapes;
- Extrusion-based techniques: a filament of material is extruded by a robot-controlled nozzle; methods such as robocasting, fused modelling deposition (FMD) and dispense plotting belong to this group;
- Methods based on a stereolithography apparatus (SLA): these methods rely on a light beam, such as digital light processing (DLP), and laser-based systems;
- Fusing of bed powders: the particles are kept together by a binder that is deposited on the bed, as in the 3D printing, or melted, as in SLS method, if it is already in the feedstock [112], [113].

In the biomedical field, AMTs are very appealing due to their ability to produce patient-specific devices; moreover, compared to the conventional fabrication techniques, most of the time they do not involve the use of toxic solvents that might remain entrapped in the structure. The high investment cost for equipment has initially limited the widespread use of AMTs in biomedicine, but in recent years they have been made more accessible and are currently used especially in maxillo-facial surgery, as drill guides, and dentistry.

The range of biomaterials that can be processed by AMTs is very broad, from calcium phosphates and bioactive glasses to bio-polymers, living cells and drugs [114]. Processing bioactive glass powders by AMTs was pioneered in the early 2000s by Kenneth Dalgarno and

his team who performed the first SLS of bioactive glass-ceramics [115]. **Table 4** summarizes the main characteristics of currently-available AMTs.

### 5.1 Selective laser sintering (SLS)

As a direct AMT, the SLS involves just one step to create a 3D object. A CO<sub>2</sub> or a Nd: YAG laser is used to perform a scan over a bed of powders, the path of which is controlled by a computer and follows the sliced CAD model of the object. As depicted in **Figure 10**, the setup is composed of two different chambers, the laser and a scanning system. The powder feedstock is prepared in one of the chambers and then a roller transfers the materials into the other chamber, thus building the powder bed through a layer-wise approach. As soon as the roller has finished preparing the layer, the laser scans the surface, consolidating the powders.

After that, the roller builds another layer and so on [114]. SLS can involve three different methods of binding particles together, i.e. solid-state sintering, liquid-state sintering and full melting of the particles. The second one is mainly used for materials that present a difficult sintering; the last one, which is also called selective laser melting (SLM), is used for low-melting-point materials, such as metals, and allows obtaining very high levels of density.

In order to be processed by SLS, the materials must absorb light in the wavelength range of the laser and their powders must be flowable, in order to ensure a correct formation of the bed. The ideal range of particle size is between 10 and 150  $\mu\text{m}$ . Other fundamental parameters include the ones involving the laser. Laser energy density, scanning speed and the hatching distance (the distance between two lines scanned by the laser) have a great influence on the resulting pore structure. Increasing the laser energy, or decreasing the scanning speed, means that a higher amount of energy has to be transferred to the materials, thus a higher temperature is reached with obvious effects on powder sintering. The final temperature depends also on the temperature of the bed that can be set, for example, at around 150°C to

allow complete removal of environmental moisture. In most of the cases, using higher energy involves an increment of the amount of liquid phase formed, which results in facilitated sintering and, thus, denser objects. However, loss in dimensional accuracy can be an issue: if the hatch distance is too narrow, the two laser paths can overlap, affecting dramatically the pore structure and decreasing the porosity. The thickness of the layer plays a crucial role as it controls the morphology of the porosity. An optimized layer can lead to interconnected porosity and pore size suitable for bone regeneration. The thickness can influence the melting of the particles, as decreasing it means that less densification of the particles and more pores will be achieved. However, one should keep in mind that a too thick layer may result in delamination between adjacent layers. On the other hand, if the layer is too small, the roller might remove and displace previously-bonded particles [116].

Bioactive glasses are suitable to be processed by SLS for obtaining amorphous or glass-ceramic scaffolds. To the best of the authors' knowledge, the first glass scaffold based on Hench's 45S5 Bioglass<sup>®</sup>, fabricated via SLS, was prepared in 2012 by Liu *et al.* [117] who optimized the laser power in order to achieve the best sintering and densification. They found that if the laser power is increased too much, holes and big voids started to appear in the glass layer. This is due to the fact that, at high laser energy (in this case 20-30 W), the material melts and can flow through the layers below. An optimized laser power also results in optimized mechanical properties, such as fracture toughness and hardness that reach their maximum value when the glass is well sintered and the residual voids (flaws) inside the filaments are minimized. Despite the very short time of the heating process, partial devitrification of 45S5 glass to  $\text{Na}_2\text{Ca}_2\text{Si}_3\text{O}_9$  has been reported during SLS fabrication [117]. SLS technique has been proved suitable also for the manufacturing of composite scaffolds. In a recent work, Gao *et al.* [118] managed to produce a scaffold with improved mechanical properties by reinforcing the glass with graphene. They prepared the feedstock by mixing

nano-sized glass powder (sol-gel 58S glass, 58SiO<sub>2</sub>-33CaO-9P<sub>2</sub>O<sub>5</sub> mol.%), having size around 48 nm, with a solution of dispersed graphene in N-methyl-2-pyrrolidone. Graphene was added in different ratios, from 0.1 to 1.5 wt.%. The scaffolds were made by SLS in a nitrogen atmosphere for preventing oxidation. By means of several analyses, such as Raman spectroscopy, FT-IR, and TEM imaging, the researchers evaluated a good dispersion of the graphene in the glass matrix, as well as the presence of a nano-texture that could promote protein adhesions; interestingly, the nanostructure typical of sol-gel glass survived the SLS process. High mechanical properties were observed for samples containing 0.5 wt.% of graphene, while they decreased in more charged samples, probably due to local agglomeration of the carbonaceous filler. The best compressive strength was 48 MPa, well above that of the cancellous bone. Graphene also played a key role in toughening the scaffolds (a fracture toughness up to 1.9 MPa m<sup>1/2</sup> was measured by the indentation method) according to different matrix-reinforcement mechanisms that are typical of many composite materials:

- Crack bridging: it is possible that the crack manages to propagate through a graphene flock, but without breaking it. In this case, the flock holds together the two side of the crack;
- Pull-out: as in fiber-reinforced composites, graphene particles can dissipate energy by being extracted from the matrix, through the breaking of the interface with the glass;
- Crack deflection: crack deflects into a different plane when it encounters graphene, resulting in a tortuous path and more energy dissipation for crack propagation;
- the crack cannot proceed through it and is obliged to deviate from its path. A longer crack means more energy required for crack propagation, hence more energy dissipation;

- Crack tip shielding: due to the interface de-bonding, a lot of energy is required and in the vicinity of graphene the crack tip is reduced;

Furthermore, these SLS-processed 58S glass/graphene composite scaffolds exhibited apatite-forming ability *in vitro* after being immersed for 7 days in SBF [118].

Although SLS was initially developed as a direct technique, it is possible to use this method as an indirect process in order to achieve better dimensional accuracy and reduce the laser power needed. In this case, the introduction of a post-processing step can be appealing: a binder (usually a polymer) is incorporated into the feedstock and mixed with the powders; then, the laser is used to melt the binder, which can hold together the glass particles. The wettability of the materials by the binder and the dimension of the glass particles are very important parameters. Smaller glass particles might result in better mechanical properties, but more binder is needed and a good and homogeneous dispersion is difficult to obtain. The total amount of the binder influences the strength of the green body – which must be enough to withstand handling and removal of non-sintered powders –, the shrinkage and the final density of the scaffold. Indirect SLS can be used to obtain glass and glass-ceramic composite scaffolds [114]. Kolan *et al.* [119] fabricated 13-93 glass scaffolds via indirect SLS using stearic acid as a binder because it leaves almost no carbon residue and is a low-melting polymer. They optimized the process by acting on the energy density, which is the key to the correct melting of the binder and is related to other crucial parameters such as the scan speed, laser power and scan spacing according to **Equation 3**:

$$E_d = \frac{P_l}{v * d} \quad (3)$$

where  $E_d$  is the energy density,  $P_l$  the laser power,  $v$  the scan speed, and  $d$  the scan spacing.

The optimal energy density was assessed by visual inspection of scaffolds to be  $1 \text{ cal}\cdot\text{cm}^{-2}$ .

This research group was able to underline both the advantages and the disadvantages of SLS in terms of obtainable porosity. Due to the unbounded glass particles that sustain the structure, it was possible to create large features that are hard to obtain through other methods. However, it was difficult to obtain features (pores or walls) below some hundreds of micrometers. The ability to decrease the dimension of the pores relies on the dimension of the laser spot and on the possibility to remove the loose particles. The smaller feature achieved in that study was around  $300 \text{ }\mu\text{m}$ . It was reported that a certain surface roughness and the presence of small micro-pores are inherent to SLS: this can help increasing the specific surface area of the scaffold (thereby speeding up ion-exchange phenomena *in vitro* and *in vivo* and hence bioactivity [120]) and offering more anchoring points for cells (osteoblasts attach and spread preferably on micro- and nano-rough surfaces [121]). A compressive strength up to 11 MPa was obtained, which perfectly lies in the typical range of the cancellous bone [119].

## 5.2 Stereolithography

Processing methods based on a stereolithography apparatus (SLA) are probably the most powerful AMTs, being characterized by the finest resolution – commercially-available machines can print features at  $20 \text{ }\mu\text{m}$  while making big objects – and capable to process a lot of different materials, from polymers and ceramics/glasses to hydrogels and cells. SLA involves the use of a liquid UV-light curable polymer stored in a tank, a UV-laser, a dynamic mirror system and a movable platform. The laser beam is patterned on the surface of the bath in order to cure the polymer on the surface and build the first layer of the object. Then, the platform moves downwards, allowing the more viscous polymer to cover the material

previously cured. The laser scans again the surface, building the next layer, and so on. Even if most of the SLA use the same mechanism as the first from Hull, and are known as bottom-up systems, another type of machine has come out, following a top-down approach (**Figure 11**).

In the second generation, the polymer is illuminated from the bottom of the vessel, which has to be transparent, and the platform moves upward. Compared to the early approach it has several advantages, such as no need for recoating of the surface, protection from oxidation (since the object is immersed), and smaller amount of feedstock [122].

A novel kind of illumination method has been recently developed that is very promising in order to greatly reduce the processing time. In the digital light projection (DLP) systems, a digital mirror device (DMD) is used to illuminate, usually with visible blue light, and reproduce every single layer at once, without the need for a beam scanning the surface (**Figure 11**). The DMD is composed of millions of mirrors that can be switched on/off in order to recreate a 2D array of pixels. In this way, the only time needed to build a layer is the one related to the exposure of the materials. Moreover, it has a great lateral resolution, about 40  $\mu\text{m}$ , and allows the use of inks with a high solid load of ceramic/glass particles (40-60%). The main problem that occurs with ceramic-filled inks is the high viscosity that reduces the capability of the ink itself to recoat the surface of the bath in the top-down approach. DLP-based systems were used to manufacture 45S5 Bioglass<sup>®</sup> scaffolds with various porous structures (**Figure 12**); in general, the “correct” slurry formulation was highlighted to be the key for the successful production of flawless scaffolds [123], [124].

A couple of advanced variations of basic SLA methods have been developed over the last decade. The micro-SLA ( $\mu\text{SLA}$ ) uses a single photon beam in order to increase the resolution and decrease the layer thickness under 10  $\mu\text{m}$ . Hydroxyapatite scaffolds with interconnected pores showing a dimension around 300  $\mu\text{m}$  had been made by this technique [125]. The other type of advanced SLA is the so-called two-photon polymerization (TPP). By using a near-

Accepted Article

infrared ultra-short-pulsed laser and a radical quenching system, features at the nano-level have been reached. The method is based on the almost simultaneous absorption of two photons by the photoinitiator. Even if the photons have low intensity, this mechanism allows enough energy to be transferred to start the polymerization. Moreover, this technique is ultra-rapid and potentially allows quick mass production. Both  $\mu$ SLA and TPP have not been experimented yet to fabricate bioactive glass scaffolds, and relevant feasibility studies would indeed deserve to be carried out in the next future.

One of the main limitations of SLA is the quite low availability of photo-curable resins. In order to obtain a sufficiently low viscosity of the resin coupled with the ability of solidifying as soon as possible after irradiation with light, the most commonly-used compositions include monomers or low-weight oligomers with several functional groups. However, these types of resins usually turned out in brittle, glassy and rigid materials. Elastomeric and biodegradable resins show promise and are under constant development.

Polymer/ceramic (glass) composites can be made by mixing the resin with ceramic particles. In order to obtain a good result, the total amount of ceramic fillers cannot be more than about 50 wt.% and the particles must be smaller than the layer thickness. Full ceramic artifacts can be created provided that the polymeric phase burns-out without leaving back any organic residues. In order to overcome the disadvantages of a low percentage of ceramic particles in the resins, an indirect method have been developed by merging SLA with gel-casting. First, an epoxy model is manufactured using SLA, then it is filled with a ceramic (glass) slurry and removed by thermal treatment. Li *et al.* [126] produced 45S5 Bioglass<sup>®</sup> scaffolds by using this technique: they first made the negative of the scaffold by SLA, using a commercial photo-curable resin, and then filled it with a slurry containing 45S5 glass powder, water and polyacrylamide; a final thermal treatment allowed the removal of the binder and the sintering of the inorganic particles. Micro-tomographic investigations showed that the resulting 45S5-

based glass-ceramic scaffold was almost an exact negative replica of the polymeric template (**Figure 13**), except for some normal shrinkage. The compressive strength (12 MPa) was found higher compared to other scaffolds obtained by direct photo-curing of a ceramic-filled resin. Furthermore, the bioactive behavior of the starring 45S5 Bioglass<sup>®</sup> was retained as demonstrated by the formation of a surface hydroxyapatite layer on scaffold struts after immersion in SBF [126].

### **5.3 Direct ink writing**

Many different AMTs can be stored under the family of the direct ink writing (DIW) (or direct ink assembly) methods. They all are based on the use of a computer-controlled translation stage to move a pattern-generating device, for example a print-head or a nozzle, to build-up an object with predetermined structure and features. Two different approaches can be used, i.e. droplet-based or continuous (“filamentary”) deposition. The former involves the use of an ink-jet print head that deposits the materials on the chosen path; methods such as 3D printing (3DP) and ink-jet printing (IJP) belong to this class. The “filamentary” techniques are based on the use of a nozzle to extrude a continuous filament of ink; they are known under several names such as robocasting, dispense plotting, extrusion free-forming or direct-write assembly.

#### *5.3.1 3D printing (3DP)*

The 3DP technique has a very similar setup compared to the SLS. In fact, it is first necessary to create a powder bed that can be moved downward by using a set of blades or rollers. Then, in order to create the layer of the object in printing, a binder is patterned by a print head following a CAD model. The print head works in the same way as a common ink-jet printer

does; it can be a continuous ink-jet printing (CIJ) or a drop-on-demand (DOD) one. In the first case, the head produces a continuous flow of ink through a nozzle from which drops are generated by acoustic waves and then deviated by means of an electric field; in the DOD system, the drop is generated only when needed by a piezoelectric or a thermal system. The type of printer has a great influence on choosing and designing the ink. Usually, the binder is water-based, but it can be also organic-based. When the layer is completed, the powders are subjected to heating in order to dry it out and consolidate it. Then, it is moved downward and another powder layer is spread in place; this cycle is repeated until the object is fully built (**Figure 14**). Afterwards, a process called de-powdering needs to be done in order to remove the loose powder: it is a crucial step in the production of porous scaffolds as special care must be paid to avoid accidental crack formation in the green body. In most cases, a final thermal treatment has to be performed to burn-out the binder and sinter the ceramic (glass) powders.

There are several parameters to control in order to obtain a good final scaffold. Before starting the actual printing, parameters of the powder bed and ink delivery system must be optimized. Since powders are transferred from a feed bed to the printing one, they must have good flowability and good packing ability. These aspects are mainly controlled by particle shape, roughness, size and size distribution. Round particles are generally better than irregular ones as they allow closer packing. Greater dimensions mean more flowability but low resolution. Powder features also influence the layer thickness. Thicker layers need more binder, while thinner ones may result in bad resolution due to the flow of the binder [112]. Usually, particles between 20 and 40  $\mu\text{m}$  are used; larger particles lead to the formation of voids and smaller ones decrease the resolution, since the binder is spread across the powder bed by capillary forces [114].

Other important parameters are the ones related to the ink drops. The drop volume and saturation of the binder are related to the packing density. The saturation is given by merging data on the packing density and the drop volume and it controls the “strength” of the green body. Wettability of the powders has a crucial effect, too: high values of it result in low resolution, while poor wettability can lead to poor binding [112].

In the field of bone tissue engineering, 3DP is very promising for the manufacturing of strong glass-derived scaffolds with a porosity around or above 50 vol.%. Various kinds of glasses and glass-ceramics have been tested, using composite powder or glass particles (then added with a binder) as starting feedstock. Crystalline phase(s) may be obtained during the scaffold sintering. The most common bioactive materials used to produce 3D-printed scaffolds are hydroxyapatite and other kinds of calcium phosphates, 45S5 Bioglass<sup>®</sup>, 13-93 glass and mesoporous bioactive glasses (MBGs). They all proved to be suitable for load-bearing applications, with compressive strength up to about 70 MPa, but the porosity is usually low (<50 vol.%) [114]. Very recently, Mancuso *et al.* [127] demonstrated the possibility to manufacture porous silicate glass-ceramic scaffolds with mechanical properties matching those of cortical bone and with dimensions of several centimeters. For this purpose, two different types of glasses (NCL2 and NCL7) with very complex compositions were used (P, B, Na, Ca, K, Mg, Mn, Al, Fe, Li, Mo, Se, Cr were added as network modifiers to the former SiO<sub>2</sub>). A so large amount of oxides was introduced to properly tailor the thermal properties and crystallization behavior of the scaffolds. Glass powders in the range of 20 to 53 μm were used and mixed with maltodextrin as a solid binder. The liquid binder, jetted by the printer, was a commercial one. The sintering process was properly adjusted to obtain a flexural strength around 36 MPa, suggesting the suitability of these scaffolds for load-bearing applications. The major drawback of these porous structures was the low total porosity,

ranging from 15 to 33 vol.%; however, macro-pores were interconnected and lied in the right size range for bone substitution (150-400  $\mu\text{m}$ ) [127].

### 5.3.2 Ink-jet printing (IJP)

The ink-jet printing (IJP) is a technique based on the disposing of ink droplets to create an object layer-by-layer. IJP is similar to 3DP and the main difference is in the ink. In 3DP, the ink is composed only by the binder and the ceramic (glass) particles are contained in the building bed; on the contrary, in IJP all the components are included in the ink. The mechanisms of the print head are the same as the ones used in the CIJ or DOD. The key advantage of IJP is the spatial accuracy on the x-y plane, up to 10  $\mu\text{m}$  vs. 25-50  $\mu\text{m}$  for DOD.

The precision of the process is affected by the physical and chemical properties of the ink: for example, viscosity and surface tension rule the way the droplets are formed and their shape, both at the exit of the nozzle and on the substrate. The wettability of the substrate by the ink, its surface tension and the interaction between droplets are the main concerns for the precision of IJP systems. For 3D objects, the solidification and consolidation stage of the ink is fundamental. Either it happens due to solvent evaporation, temperature change, gelling or photo-curing, that step will determine the final shape of the object.

IJP is a very powerful technique in the field of tissue engineering since it allows a wide range of materials to be printed. To date, IJP has been used to fabricate scaffolds based on natural (e.g. agar, alginate, cellulose) and synthetic polymers (e.g. poly (lactic acid), poly (caprolactone), hydrogels) as well as on calcium phosphates (e.g. hydroxyapatite and tri-calcium phosphates) [128]. Since hard ceramics cannot be processed in a molten state due to their high melting temperature, they are mixed with a binder to obtain a suitable ink; a thermal treatment is added at the end of the process to remove the binder and sinter the

ceramic particles. Several nozzles can be used in IJP at the same time, in order to reduce the time of printing a single layer and obtain composites by using different inks [129]. Despite these attractive characteristics, no reports on glass-based IJ-printed scaffolds have been found in the literature.

### 5.3.3 Robocasting

Robocasting is perhaps the most common and powerful direct ink writing technique based on the continuous extrusion of a filament [114]. Other similar approaches are the fusion deposition modelling, where a molten paste is extruded through a nozzle, or the micro-pen writing that is not suitable to print ceramics [130]. All these techniques are based on the ink being extruded by a nozzle, using pressurized air, in order to produce a rod that is deposited by a computer-controlled head, which usually follows a CAD file. A scheme of the robocasting set-up is represented in **Figure 16**.

Robocasting is dependent on the availability of inks with very specific properties. The ink is a slurry, composed of glass or ceramic particles and a polymeric binder, to form a colloidal suspension. The requirements that a “good ink” must provide were discussed by Cesarano *et al.* [131] in 1999 and are still valid. In order to be used as robocasting ink, a colloidal slurry should:

- Be pseudo-plastic. In fact, the ink has to flow through a small nozzle, but without applying too much pressure;
- Set-up into a non-flowable mass. It has to maintain the rod-like structure even after the dispensing on the building surface;
- It has to be strong enough to bear the weight of the overlying layers without undergoing any deformation.

A colloidal ink is prepared by mixing colloidal particles in an aqueous mean, then polyelectrolytes with ionizable groups (e.g. poly(acrylic acid)) are usually added as dispersants to provide stability. Changes in pH, temperature or other conditions provoke changes in the surface charge that influence the stability of the suspension and lead to the fluid-gel transition [132].

In rheology science, a pseudo-plastic fluid is a liquid that has a shear-dependent viscous behavior. When a fluid is subjected to a shear stress,  $\tau$ , the shear rate,  $\dot{\gamma}$ , is related to  $\tau$  by the following relationship: (**Equation 4**):

$$\tau = \tau_y + \eta \times \dot{\gamma}^n \quad (4)$$

where  $\eta$  is the viscosity,  $n$  is the characteristic exponential coefficient, and  $\tau_y$  is the yielding stress, which may also be equal to zero and is the minimum stress value necessary to observe the flow of the fluid. A material that follows **Equation 4** is known as a Herschel-Bulkley material [132].

There are three classes of fluids, sorted by their viscous behavior, defined by the value of their coefficient  $n$ :

- Newtonian fluids,  $n = 1$ : they have a constant deformation, independent on the shear applied;
- Pseudo-plastic or shear-thinning fluids,  $n < 1$ : the shear stress increases with decreasing slope as the shear rate rises;
- Dilatant or shear-thickening fluids,  $n > 1$ : the shear stress slope increases with increasing shear rate [133].

The robocasting building principle relies on the ability of the ink to change its viscosity, through physical and/or chemical processes, in order to become strong enough to support the on-building structure. Cesarano *et al.* [131] achieved the transition between a pseudo-plastic fluid and a dilatant one, and so the strength needed, by drying of the rods: thus, a change

(increase) in the particle volume fraction leads to a change in the ink rheology. One of the drawbacks of extruding directly in the air is the possibility of uneven shrinkage, due to different air flows in the structure. In order to avoid this problem and print finer features, the use of a non-wetting oil bath as printing environment has been reported. Thus, the drying is avoided and shape retention is obtained by recovery of the gel elasticity; then, the oil is removed and the structure is dried in a controlled environment. An additional advantage of this approach, although it may be technically challenging, is to avoid clogging of the nozzle. In the air, it is also necessary to coordinate the feed rate with the drying kinetics, thus allowing previous layers to get enough strength: this problem is overcome by extruding in oil. On the other hand, it is always mandatory to control the viscoelastic behavior of the ink as well as its ability to “fuse” with the underlying rods.

The first aim in ink preparation is to achieve a stable dispersion and a solid loading (i.e. the fraction of ceramic or glass particles) as high as possible in order to reduce the drying shrinkage; then, the fluid-to-gel transition is promoted by a physical or chemical change in the system.

The rheology of the gelled ink is important during the extrusion process and the actual printing phase. There are two main delivery systems for ink in robocasting:

- Constant-displacement: the ink is injected at a constant flow rate by mechanically displacing the plunger of the cartridge through varying the pressure as needed;
- Constant-pressure: the plunger is moved by pressurized air that it is maintained at a constant pressure [130].

The latter method has a simpler set up, but the material feed might not be constant if the rheology of the ink changes during the process. The shear stress applied to the ink varies with the distance from the axis of the nozzle according to **Equation 5**:

$$\tau_r = \frac{r\Delta P}{2l} \quad (5)$$

where  $\tau_r$  is shear stress at the position  $r$  (distance from the center of the nozzle),  $\Delta P$  is the pressure gradient applied, and  $l$  is the nozzle length.

A Herschel-Bulkley material that flows through a nozzle may generate a three-velocity zones profile due to the stress gradient, i.e. a central core of non-yielded materials, which is in gel state and flows at a constant velocity; an intermediate layer of yielded materials, which is in fluid state and exhibits a laminar flow; and an external slip fluid layer, attached to the nozzle walls, which is depleted of colloidal particles. This situation leads to an overall plug flow of the ink; the larger is the nozzle, the smaller is the effect of the laminar zone.

Once the rod is deposited on the layer lying underneath, it is important that the ink exhibits enough mechanical strength in order to support the new to-build layer without undergoing large deformation and maintain the shape of the as-deposited structure. In fact, if the ink is too “weak”, it might bend between two lines of the underlying layer [134].

The elastic properties of the ink can be controlled by tuning the attractive forces between the ceramic or glass particles that form the colloidal suspension. A colloidal gel is capable to transfer loads if a critical volume fraction of colloidal particles is reached. This fraction,  $\varphi_{gel}$ , is known as gel point and it is inversely proportional to the attractive forces among particles.

For a certain colloidal gel of constant volume fraction,  $\varphi$ , above the gel point, an elastic property,  $y$ , can be obtained by **Equation 6**:

$$y = k \left( \frac{\varphi}{\varphi_{gel}} - 1 \right)^x \quad (6)$$

where  $k$  is a constant and  $x$  is a scaling exponent, usually of value around 2.5. This relationship allows obtaining elastic properties of the material, such as shear modulus  $G$  and shear yield stress  $\tau_y$ . For an ink of given  $\varphi$ , increasing the attractive forces among particles

means a reduction of the gel point and, thus, an increment of the mechanical properties of the ink [132].

Along with the intrinsic properties of the ink, there are several other factors that influence the final outcome of the printing process. The final diameter of the extruded rod is determined not only by the diameter of the nozzle but also by the pressure of the air and by the printing velocity. These two parameters have to be contemporaneously adjusted to obtain a constant shape. If the pressure is too low or the speed too high, the elastic recovery of the ink will cause breakdowns of the lines due to a lack of materials. On the other hand, if there are too much pressure and too slow movement, the rods will be large and deformed, thereby provoking a loss of the structural features. The spacing along the z-axis is fundamental to achieve a good adhesion between the layers and avoid delamination or loss in mechanical properties: in fact, it should be not too great, thus letting the rods adhere to the underlying layers, and not too little, thereby avoiding deformation of the extruding rod and the lines underneath. The printing substrate plays also a crucial role: in fact, it has to be perfectly plane and should allow attachment during printing, in order to “block” the structure and avoid any unwanted movements; furthermore, detachment of the completed and dried object from the substrate should be easy and neat to avoid any damage. Since robocasting allows printing features in the range of a few micrometers, even micrometrical deviations from the planarity in the printing substrate may lead to defects.

The robocasting technique was first used for producing bioceramic scaffolds for bone regeneration by Franco *et al.* in 2010 [135]. They developed a hydrogel-based ink containing calcium phosphates (hydroxyapatite and  $\beta$ -TCP) and print it using nozzle diameters ranging from 100 to 250  $\mu\text{m}$ . In their work, they highlighted the effect of the grain size distribution and proposed Pluronic, a surfactant block co-polymer (polyethylene oxide (PEO)–propylene oxide (PPO)–polyethylene oxide (PEO)), as a dispersant to form the colloidal ink. The use of

a large distribution of powder size allows increasing the volume of the particles loaded within the ink, because the smaller particles promote the rearrangement of the bigger ones, thus facilitating the slip of the ink. This leads to a lower pressure needed for the extrusion and to the possibility of using nozzles with smaller diameters. Moreover, the use of a conical tip prevents the formation of dead zones inside the nozzle, avoiding its clogging [135].

Pluronic was also used by Fu *et al.* for the production of the first bioactive glass (13-93)-based robocast scaffold [136]. Pluronic F-127 is one of the three most commonly-used binders for robocasting in bone applications, along with ethyl cellulose/polyethylene glycol and carboxymethyl cellulose. The last two are processed in ethanol instead of water, which is used for F-127. Thus, early ionic dissolution of the glass is prevented, but the control of the whole process is much more difficult. For example, the robocasting must be performed in a controlled chamber, within an ethanol-rich environment to prevent evaporation [137]. No organic residues of the binder are left in the scaffold after the thermal treatment (sintering), and no other chemicals or products are used that can be toxic for the human body.

F-127 has a thermally-reversible fluid-gel transition due to water adsorption/desorption capacity of the PPO block due to the presence of hydroxyl groups. At a temperature around 0°C, Pluronic forms a liquid solution in water because it adsorbs on the polymer, extending the chains and making them to slide across each other. When the temperature rises up to 40°C, the adsorption of water is energetically unfavorable and the polymeric chains form micelles and the solution changes from a fluid state to the gel one [138]. If glass particles are dispersed in the solution, Pluronic stabilizes them sterically by generating Van der Waals or hydrogen bonding with the surface of the particles using the hydroxyl groups in the polymeric chains [136]. It was observed that the presence of glass particles inside the Pluronic suspension lowers the temperature at which the state transition takes place. This is due to a preferential bonding of water to glass than to the Pluronic. In this way, water is

subtracted from the F-127 much earlier than what would happen in a pure Pluronic-water solution. F-127-based inks offer the advantages to be printed directly in air, making much easier the whole process.

45S5 Bioglass<sup>®</sup>-based robocast scaffolds were recently produced by Motealleh *et al.* [139], who used carboxymethyl cellulose as a binder and studied the effects of different post-processing thermal treatments on scaffold properties. Both amorphous and highly-crystallized scaffolds retained the proper CAD-derived geometry (**Figure 17**) and apatite-forming ability after sintering, but the latter ones obviously exhibited higher mechanical properties (compressive strength: 11 vs. 2 MPa; strain energy density (toughness): 0.3 vs. 0.03 MJ/m<sup>3</sup>).

In order to print in a non-wetting oil bath, the printer set-up is more complicated because it needs a tank to contain the oil and often also the possibility of heating it. Moreover, the printing substrate is a multilayered structure, composed of a basic layer and two soluble ones.

Franco *et al.* [135] used an alumina sheet coated by an oil-soluble layer and a top one made of corn syrup, which is oleophobic. When the structure is printed on the corn syrup layer, the water inside the ink starts to dissolve the top layer, exposing the oil-soluble one to the oil.

When also the mid layer is dissolved, the printed structure detaches easily from the alumina plate [135]. A similar method was also used by Fu *et al.* to robocast high-strength 13-93 glass scaffolds [136]. Substrates for printing in the air can be composed of only one layer: for example, Nommeots-Nomm *et al.* [138] used commercial acetate sheets that are perfectly flat, cheap and allow easy detachment of the printed structures after drying.

Robocasting has been proved as a very valuable method for the fabrication of glass scaffolds for bone application, even for load-bearing sites. Using particle size ranging from 30  $\mu\text{m}$  down to 1  $\mu\text{m}$  and extrusion nozzles with diameters between 100 and 580  $\mu\text{m}$ , it is possible to obtain glass structures having total porosity within 50-70 vol.% and pore dimensions varying from few hundreds of micrometers up to half a millimeter. Robocast glass scaffolds can

exhibit considerably high compressive strength, in most cases higher than that of cancellous bone (from 13 to 142 MPa, which is even higher than the strength of cortical bone [138]).

Robocasting offers a very easy control of the structure of the scaffolds, also giving the opportunity to create functionally-graded porous devices. Mattioli-Belmonte *et al.* [140] used a robocasting system, called pressure-assisted micro-syringe (PAM), to produce bioactive glass/poly(lactic-co-glycolic acid) (PLGA) 2D porous structures with a well-defined topology which were then assembled layer by layer to build-up 3D bone-like scaffolds replicating tomographic reconstructions of human bone [140]. These glass/PLGA composite structures exhibited an elastic modulus comparable to that of cancellous bone and induced the osteoblastic differentiation of human periosteal precursor cells, therefore showing great promise for bone tissue engineering applications.

Robocasting has recently shown great promise for the fabrication of hierarchical scaffolds based on MBGs, which exhibit an inherent texture of ordered mesopores (2-50 nm) making the material highly brittle. Over the last decade, MBGs have been proposed as novel implantable platforms for the local release of a number of therapeutic agents, including inorganic ionic dissolution products, drugs and growth factors [141]. However, the size of meso-pores is several orders of magnitude smaller than bone cells (10-200  $\mu\text{m}$ ), which precludes cells from entering the implant meso-pores. Hence, MBGs should be somehow processed by macro/meso-co-templating strategies to acquire macroscale porosity allowing bone cell penetration, adhesion to the scaffold struts and proliferation, as well as new tissue ingrowth [142]. Scaffold processing methods should also preserve the original meso-porosity of MBGs, which is the key for encapsulating and releasing therapeutic biomolecules. Initially, hierarchical MBG scaffolds were produced by dipping a macro-cellular template (e.g. a polymeric sponge) into the sol, but dramatically brittle structures were obtained (compressive strength in the range of 50 to 250 kPa) [143]. A tremendous improvement was

obtained by applying robocasting to MBGs, as illustrated in **Figure 15**. After the early feasibility trials on SiO<sub>2</sub>-P<sub>2</sub>O<sub>5</sub> MBGs [144], Wu *et al.* [145] robocast SiO<sub>2</sub>-CaO-P<sub>2</sub>O<sub>5</sub> MBG powders using poly(vinyl alcohol) as a binder and obtained macro-mesoporous scaffolds with a compressive strength of 16 MPa, along with excellent mineralization ability and sustained drug release property. Robocast MBG scaffolds were also shown to retain good mechanical strength (7 MPa) after being soaked in SBF to mimic their evolution upon contact with body environment [146].

A valuable picture on AMTs applied to bioceramics and MBGs for producing hierarchical scaffolds was recently provided by Ma *et al.* [147].

## **6. BIOFABRICATION: TOWARDS MULTIPLE-TISSUE ENGINEERING AND ORGAN REGENERATION**

The emergence of biofabrication brings high hopes for the generation of constructs that more closely recapitulate the complexity and heterogeneity of various tissues and organs [148].

Based on the definition, biofabrication refers to “the automated generation of biologically functional products with the structural organization from living cells, bioactive molecules, biomaterials, cell aggregates such as micro-tissues, or hybrid cell-material constructs, through bioprinting or bioassembly and subsequent tissue maturation processes” [149]. AMTs can open new horizons in the emerging field of biofabrication, which combines biomaterials, biomolecules and living cells as building blocks to print tissues and whole organs [150].

Looking at the future, the last frontier of AMTs applied to biofabrication is the simultaneous regeneration of multiple tissues by producing functionally-graded scaffolds. Early experiments on the layer-wise production of heterogeneous organs (outer ear, kidney and tooth) by using multi-head printing systems have been recently reported [151]; this strategy is

currently limited to print soft matter (polymeric hydrogels and cells), but incorporation of “rigid” bioactive glass inclusions could be possible after some technological optimizations in the next future. In this regard, IJP and robocasting show great promise as they allow the use of multiple printer heads/nozzles for depositing various biomaterials during the same printing cycle with a high degree of versatility. Of course, the risk of mechanical damage to the delicate cellular structure by hard bioactive glass particles should be taken into careful account, and the use of nano-sized bioactive glass could be suggested to minimize this problem.

An interesting, early example of interfacial tissue engineering involving bioactive glasses was reported by Liverani *et al.* [152], who prepared multilayered scaffolds (porous bioactive glass scaffold + interfacial polymeric region + chitosan/alginate soft layer) for osteochondral tissue engineering by combining foam replication, freeze-drying, and electrospinning (**Figure 18**).

More recently, Murphy *et al.* [153] prepared a 3D bioprinted construct of stem cells and polymer/bioactive glass for bone tissue engineering applications. The main idea behind this study was to take advantage of the angiogenic capability of borate-based bioactive glasses to make a construct with the ability to improve tissue regeneration. For this aim, borate glasses (at the concentration of 10 to 50 wt.%) were added to a mixture of PCL and an organic solvent to make an extrudable paste. Furthermore, the authors suspended adipose-derived stem cells (ASCs) in Matrigel and ejected them as droplets using the second syringe. They could successfully fabricate 10 mm × 10 mm × 1 mm scaffolds with pore sizes ranging from 100 to 300 μm; the constructs showed a good bioactivity when immersed in culture media for up to two weeks. The viability assay showed more than 60% viable ASCs on the scaffold at one week after incubation.

Additive manufacturing of bioactive glasses has the potential to meet these technological, clinical and social challenges and to further expand the applications of biomedical glasses from the restoration of bone and teeth to the repair of soft tissues [154], [155], thus contributing – citing L.L. Hench’s words – “to cope with the problems of a world that has finite resources but infinite desires” [156].

## 7. CONCLUSIONS

Over the last decade, there have been tremendous advances in the field of manufacturing of bioactive glass and ceramic scaffolds for tissue engineering applications. Perhaps sponge replication still remains the most popular, easiest and cheapest method to produce 3D ceramic structures that closely resemble trabecular bone, but suffers from some limitations such as process reproducibility and capability to fabricate large and complex porous bodies. AMTs allow a better control of scaffold geometry and pore/strut characteristics, as well as an obvious scalability to the industrial level. Some AMTs, like SLS, still require high investment costs but simple 3D printers have recently been made relatively accessible and can be designed and even built in-house for customized applications. However, it cannot be ignored that the production of highly-porous scaffolds with porosity >70 vol.%, and more specifically bone-like structures made of thin struts (from few micrometers to few tens of micrometers), still remains a challenge when AMTs are used. In most cases, scaffolds obtained by AMTs are limited to porous structures consisting of large rods or struts/walls with size >40-50  $\mu\text{m}$  due to the inherent resolution of AMTs, even with the most performing equipment. The last frontier of scaffold manufacturing is biofabrication, which allows simultaneous printing of biomaterials, biomolecules and living cells, thus opening new horizons towards the regeneration of multiple tissues and whole organs.

## REFERENCES

1. Johnell O, Kanis J. An estimate of the worldwide prevalence and disability associated with osteoporotic fractures. *Osteoporos Int.* 2006;17:1726.
2. Klifto C, Gandi S, Sapienza A. Bone graft options in upper-extremity surgery. *J Hand Surg Am.* 2018;43(8):755-761.
3. Miller C, Chiodo C. Autologous bone graft in foot and ankle surgery. *Foot Ankle Clin N Am.* 2016;21:825-837.
4. Loi F, Córdova LA, Pajarinen J, Lin T hua, Yao Z, Goodman SB. Inflammation, fracture and bone repair. *Bone.* 2016;86:119-130.
5. Conzemius M, Swainson S. Fracture fixation with screws and bone plates. *Vet Clin North Am Small Anim Pract.* 1999;29:1117-1133.
6. Lasanianos NG, Kanakaris NK, Giannoudis P V. Current management of long bone large segmental defects. *Orthop Trauma.* 2010;24(2):149-163.
7. Campana V, Milano G, Pagano E, Barba M, Cicione C, Salonna G. Bone substitutes in orthopaedic surgery. *J Mater Sci Mater Med.* 2014;25:2445-2461.
8. Giannoudis P V., Dinopoulos H, Tsiridis E. Bone substitutes: An update. *Injury.* 2005;36(3):S20-S27.
9. Moore WR, Graves SE, Bain GI. Synthetic bone graft substitutes. *ANZ J Surg.* 2001;71(6):354-361.
10. Baino F, Vitale-Brovarone C. Three-dimensional glass-derived scaffolds for bone tissue engineering: Current trends and forecasts for the future. *J Biomed Mater Res - Part A.* 2011;97 A(4):514-535.
11. Schlickewei W, Schlickewei C. The use of bone substitutes in the treatment of bone defects - the clinical view and history. *Macromol Symp.* 2007;253:10-23.

12. Baino F. Ceramics for bone replacement: commercial products and clinical use. In: Palmero P, Cambier F, De Barra E, eds. *Advances in Ceramic Biomaterials*. Duxdorf (UK): Woodhead Publishing (Elsevier); 2017:249-278.
13. Hutmacher DW. Scaffolds in tissue engineering bone and cartilage. *Biomaterials*. 2000;21:2529-2543.
14. Dorozhkin SV. Calcium orthophosphate-based bioceramics. *Materials (Basel)*. 2013;6:3840-3942.
15. Velasco MA, Narváez-Tovar CA, Garzón-Alvarado DA. Design, materials, and mechanobiology of biodegradable scaffolds for bone tissue engineering. *Biomed Res Int*. 2015;2015(August 2016).
16. Fu Q, Saiz E, Rahaman MN, Tomsia AP. Bioactive glass scaffolds for bone tissue engineering: State of the art and future perspectives. *Mater Sci Eng C*. 2011;31(7):1245-1256.
17. Hench LL. The story of Bioglass. *J Mater Sci Mater Med*. 2006;17:967-978.
18. Jones JR, Brauer DS, Hupa L, Greenspan DC. Bioglass and bioactive glasses and their impact on healthcare. *Int J Appl Glas Sci*. 2016;7:423-434.
19. Balasubramanian P, Büttner T, Miguez Pacheco V, Boccaccini AR. Boron-containing bioactive glasses in bone and soft tissue engineering. *J Eur Ceram Soc*. 2018;38:855-869.
20. Abou Neel EA, Pickup DM, Valappil SP, Newport RJ, Knowles JC. Bioactive functional materials: a perspective on phosphate-based glasses. *J Mater Chem*. 2009;19:690-701.
21. Shah R, Ready D, Knowles JC, Hunt NP, Lewis MP. Sequential identification of a degradable phosphate glass scaffold for skeletal muscle regeneration. *J Tissue Eng Regen Med*. 2014;8:801-810.

22. Kim YP, Lee GS, Kim JW, Kim MS, Ahn HS, Lim JY, et al. Phosphate glass fibres promote neurite outgrowth and early regeneration in a peripheral nerve injury model. *J Tissue Eng Regen Med.* 2015;9:236-246.
23. Rabiee SM, Nazparvar N, Azizian M, Vashae D, Tayebi L. Effect of ion substitution on properties of bioactive glasses: A review. *Ceram Int.* 2015;41:7241-7251.
24. Kargozar S, Baino F, Hamzehlou S, Hill RG, Mozafari M. Bioactive glasses: sprouting angiogenesis in tissue engineering. *Trends Biotechnol.* 2018;36:430-444.
25. Kargozar S, Baino F, Hamzehlou S, Hill RG, Mozafari M. Bioactive glasses entering the mainstream. *Drug discov Today.* 2018; 23:1700-1704.
26. Kargozar S, Montazerian M, Hamzehlou S, Kim HW, Baino, F. Mesoporous bioactive glasses: promising platforms for antibacterial strategies. *Acta Biomater.* 2018; 81: 1-19.
27. Kargozar S, Mozafari M, Hill RG, Brouki Milan P, Taghi Joghataei M, Hamzehlou S, et al. Synergistic combination of bioactive glasses and polymers for enhanced bone tissue regeneration. *Mater Today Proc.* 2018;5:15532-15539.
28. Chen Q, Baino F, Spriano S, Pugno NM, Vitale-Brovarone C. Modelling of the strength-porosity relationship in glass-ceramic foam scaffolds for bone repair. *J Eur Ceram Soc.* 2014;34(11):2663-2673.
29. Liang S-L, Cook WD, Thouas GA, Chen Q-Z. The mechanical characteristics and in vitro biocompatibility of poly (glycerol sebacate)-bioglass® elastomeric composites. *Biomaterials.* 2010;31:8516-8529.
30. Hasson CJ. Foreign body reaction to biomaterials. *Semin Immunol.* 2009;27:590-609.
31. Henkel J, Woodruff MA, Epari DR, Steck R, Glatt V, Dickinson IC, et al. Bone regeneration based on tissue engineering conceptions — a 21st century perspective. *Bone Res.* 2013;1(3):216-248.

32. Velard F, Braux J, Amedee J, Laquerriere P. Inflammatory cell response to calcium phosphate biomaterial particles: An overview. *Acta Biomater.* 2013;9(2):4956-4963.
33. El-Rashidy AA, Roether JA, Harhaus L, Kneser U, Boccaccini AR. Regenerating bone with bioactive glass scaffolds: A review of in vivo studies in bone defect models. *Acta Biomater.* 2017;62:1-28.
34. Reznikov R, Shahar R, Weiner S. Bone hierarchical structure in three dimensions. *Acta Biomater.* 2014;10:3815-3826.
35. Simske SJ, Ayers RA, Bateman T. Porous materials for bone engineering. *Mater Sci Forum.* 1997;250:151-182.
36. Gerhardt L-C, Boccaccini AR. Bioactive glass and glass-ceramic scaffolds for bone tissue engineering. *Materials (Basel).* 2010;3(7):3867-3910.
37. Peroglio M, Gremillard L, Gauthier C, Chazeau L, Verrier S, Alini M, et al. Mechanical properties and cytocompatibility of poly( $\epsilon$ -caprolactone)- infiltrated biphasic calcium phosphate scaffolds with bimodal pore distribution. *Acta Biomater.* 2010;6(11):4369-4379.
38. Carter DR, Schwab GH, Spengler DM. Tensile fracture of cancellous bone. *Acta Orthop Scand.* 1980;51(1-6):733-741.
39. Oliveira PT De, Zalzal SF, Beloti MM, Rosa AL, Nanci A. Enhancement of in vitro osteogenesis on Ti by chemically produced nanotopography. *J Mater Sci Res A.* 2007;80:554-564.
40. Qu Z, Rausch-Fan X, Wieland M, Matejka M, Schedle A. The initial attachment and subsequent behavior regulation of osteoblasts by dental implant surface modification. *J Biomed Mater Res A.* 2007;82:658-668.
41. Feller L, Jadwat Y, Khammissa RAG, Meyerov R, Schechter I, Lemmer J. Cellular responses evoked by different surface characteristics of intraosseous Ti implants.

Biomed Res Int. 2015;2015:171945.

42. Aivelabegan HT, Sadroddin E. Fundamentals of protein and cell interactions in biomaterials. *Biomed Pharmacother.* 2017;88:956-970.
43. Wilson C, Clegg R, Leavesley D, Percy M. Mediation of biomaterial–cell interactions by adsorbed proteins: a review. *Tissue Eng.* 2005;11:1-18.
44. Chandorkar Y, Ravikumar K, Basu B. The foreign body response demystified. *ACS Biomater Sci Eng.* 2019;5:19-44.
45. Webster TJ, Siegel RW, Bizios R. Osteoblast adhesion on nanophase ceramics. *Biomaterials.* 1999;20(13):1221-1227.
46. Sepulveda P, Jones JR, Hench LL. Bioactive sol-gel foams for tissue repair. *J Biomed Mater Res.* 2002;59(2):340-348.
47. Fiume E, Barberi J, Verné E, Baino F. Bioactive glasses: from parent 45S5 composition to scaffold-assisted tissue-healing therapies. *J Funct Biomater.* 2018;9-24.
48. Roseti L, Parisi V, Petretta M, Cavallo C, Desando G, Bartolotti I, et al. Scaffolds for bone tissue engineering: state of the art and new perspectives. *Mater Sci Eng C.* 2017;78:1246-1262.
49. Jones JR. Review of bioactive glass: from Hench to hybrids. *Acta Biomater.* 2013;9:4457-4486.
50. Baino F, Hamzehlou S, Kargozar S. Bioactive glasses: where are we and where are we going? *J Funct Biomater.* 2018;9:25.
51. Wen Y, Xun S, Haoye M et al. 3D printed porous ceramic scaffolds for bone tissue engineering: a review. *Biomater Sci.* 2017; 22: 1690-1698.
52. Filho OP, Latorre GP, Hench LL. Effect of crystallization on apatite-layer formation of bioactive glass 45S5. *J Biomed Mater Res.* 1996;30(4):509-514.

53. Fagerlund S, Massera J, Moritz N, Hupa L, Hupa M. Phase composition and in vitro bioactivity of porous implants made of bioactive glass S53P4. *Acta Biomater.* 2012;8(6):2331-2339.
54. Massera J, Mayran M, Rocherullé J, Hupa L. Crystallization behavior of phosphate glasses and its impact on the glasses' bioactivity. *J Mater Sci.* 2015;50(8):3091-3102.
55. Rahaman MN. *Ceramic processing and sintering.* 2nd ed. Boca Raton: CRC Press; 2003.
56. German RM, Suri P, Park J. Review: liquid phase sintering. *J mater Sci.* 2009;44:1-39.
57. Kang S-JL. *Sintering: densification, grain growth and microstructure.* 1st ed. Butterworth-Heinemann: Elsevier Butterworth-Heinemann; 2005.
58. De Jonghe LC, Rahaman MN. Sintering of ceramics. In: *Handbook of Advanced Ceramics: Materials, Applications, Processing and Properties.* Elsevier Ink; 2003:187-264.
59. Chen Q, Mohn D, Stark WJ. Optimization of Bioglass® scaffold fabrication process. *J Am Ceram Soc.* 2011;94:4184-4190.
60. German RM, Farooq S, Kipphut CM. Kinetics of liquid sintering. *Mater Sci Eng A.* 1988;105-106:215-224.
61. Ferraris M, Verné E. Viscous phase sintering of particle-reinforced glass matrix composites. *J Eur Ceram Soc.* 1996;16(4):421-427.
62. Verné E, Defilippi R, Carl G, Vitale Brovarone C, Appendino P. Viscous flow sintering of bioactive glass-ceramic composites toughened by zirconia particles. *J Eur Ceram Soc.* 2003;23(5):675-683.
63. Huang R, Pan J, Boccaccini AR, Chen Q-Z. A two-scale model for simultaneous sintering and crystallization of glass–ceramic scaffolds for tissue engineering. *Acta*

Biomater. 2008;4:1095-1103.

64. Denes E, Barrière G, Poli E, Lévêque G. Commentary: bioceramics and scaffolds: a winning combination for tissue engineering. *Front Bioeng Biotechnol.* 2017;5(December):1-17.
65. Omatete OO, Janney M a., Nunn SD. Gelcasting: from laboratory development toward industrial production. *J Eur Ceram Soc.* 1997;17(2-3):407-413.
66. Sepulveda P, Binner JG. Processing of cellular ceramics by foaming and in situ polymerisation of organic monomers. *J Eur Ceram Soc.* 1999;19(12):2059-2066.
67. Wu ZY, Hill RG, Yue S, Nightingale D, Lee PD, Jones JR. Melt-derived bioactive glass scaffolds produced by a gel-cast foaming technique. *Acta Biomater.* 2011;7(4):1807-1816.
68. Poologasundarampillai G, Lee P, Lam C, Kourkouta A, Jones J. Compressive strength of bioactive sol-gel glass foam scaffolds. *Int J Appl Glas Sci.* 2016;7:229-237.
69. Baino F, Fiume E, Miola M, Verné E. Bioactive sol-gel glasses: processing, properties and applications. *Int J Appl Ceram Technol.* 2018;15:841-860.
70. Jones JR, Ehrenfried LM, Hench LL. Optimising bioactive glass scaffolds for bone tissue engineering. *Biomaterials.* 2006;27:964-973.
71. Midha S, Kim T, Van den Bergh W, Lee P, Jones J, Mitchell C. Preconditioned 70S30C bioactive glass foams promote osteogenesis in vivo. *Acta Biomater.* 2013;9:9169-9182.
72. Jones JR, Ehrenfried LM, Saravanapavan P, Hench LL. Controlling ion release from bioactive glass foam scaffolds with antibacterial properties. *J Mater Sci Mater Med.* 2006;17:989-996.
73. Baino F, Fiume E, Miola M, Leone F, Onida B, Verné E. Fe-doped bioactive glass-derived scaffolds produced by sol-gel foaming. *Mater Lett.* 2019;235:207-211.

74. Rainer A, Giannitelli SM, Abbruzzese F, Traversa E, Licoccia S, Trombetta M. Fabrication of bioactive glass-ceramic foams mimicking human bone portions for regenerative medicine. *Acta Biomater.* 2008;4(2):362-369.
75. Navarro M, Del Valle S, Martínez S, Zeppetelli S, Ambrosio L, Planell JA, et al. New macroporous calcium phosphate glass ceramic for guided bone regeneration. *Biomaterials.* 2004;25(18):4233-4241.
76. Fu Q, Rahaman MN, Bal BS, Huang W, Day DE. Preparation and bioactive characteristics of a porous 13–93 glass, and fabrication into the articulating surface of a proximal tibia. *J Biomed Mater Res Part A.* 2007;28A:222-229.
77. Liang W, Rahaman MN, Day DE, Marion NW, Riley GC, Mao JJ. Bioactive borate glass scaffold for bone tissue engineering. *J Non Cryst Solids.* 2008;354(15-16):1690-1696.
78. Rezwan K, Chen QZ, Blaker JJ, Boccaccini AR. Biodegradable and bioactive porous polymer/inorganic composite scaffolds for bone tissue engineering. *Biomaterials.* 2006;27(18):3413-3431.
79. Livingston T, Ducheyne P, Garino J. In vivo evaluation of a bioactive scaffold for bone tissue engineering. *J Biomed Mater Res.* 2002;62(1):1-13.
80. Brovarone CV, Verné E, Appendino P. Macroporous bioactive glass-ceramic scaffolds for tissue engineering. *J Mater Sci Mater Med.* 2006;17(11):1069-1078.
81. Zhang H, Ye XJ, Li JS. Preparation and biocompatibility evaluation of apatite/wollastonite-derived porous bioactive glass ceramic scaffolds. *Biomed Mater.* 2009;4(4).
82. Lyckfeldt O, Ferreira JMF. Processing of porous ceramics by “starch consolidation.” *J Eur Ceram Soc.* 1998;18(2):131-140.
83. Vitale-Brovarone C, Vernè E, Bosetti M, Appendino P, Cannas M. Microstructural

and in vitro characterization of SiO<sub>2</sub>-Na<sub>2</sub>O-CaO-MgO glass-ceramic bioactive scaffolds for bone substitutes. *J Mater Sci Mater Med.* 2005;16(10):909-917.

84. Vitale-Brovarone C, Di Nunzio S, Bretcanu O, Verné E. Macroporous glass-ceramic materials with bioactive properties. *J Mater Sci Mater Med.* 2004;15(3):209-217.
85. Prasara J, Gheewala SH. Sustainable utilization of rice husk ash from power plants: A review. *J Clean Prod.* 2017;167:1020-1028.
86. Wu SC, Hsu HC, Hsiao SH, Ho WF. Preparation of porous 45S5 Bioglass®-derived glass-ceramic scaffolds by using rice husk as a porogen additive. *J Mater Sci Mater Med.* 2009;20(6):1229-1236.
87. Roether JA, Boccaccini AR, Hench LL, Maquet V, Gautier S, Jérôme R. Development and in vitro characterisation of novel bioresorbable and bioactive composite materials based on polylactide foams and Bioglass® for tissue engineering applications. *Biomaterials.* 2002;23(18):3871-3878.
88. Baino F, Verné E. Glass-based coatings on biomedical implants: a state-of-the-art review. *Biomed Glas.* 2017;3:1-17.
89. Fiorilli S, Baino F, Cauda V, Crepaldi M, Vitale-Brovarone C, Demarchi D, et al. Electrophoretic deposition of mesoporous bioactive glass on glass-ceramic foam scaffolds for bone tissue engineering. *J Mater Sci Mater Med.* 2015;26:21.
90. Molino G, Bari A, Baino F, Fiorilli S, Vitale-Brovarone C. Electrophoretic deposition of spray-dried Sr-containing mesoporous bioactive glass spheres on glass-ceramic scaffolds for bone tissue regeneration. *J Mater Sci.* 2017;52:9103-9114.
91. Baino F, Potestio I, Vitale-Brovarone C. Production and physicochemical characterization of Cu-doped silicate bioceramic scaffolds. *Materials (Basel).* 2018;11:1524.
92. Yu M, Fiume E, Verné E, Saunders T, Reece MJ, Baino F. Bioactive sol-gel glass-

coated wood-derived biocarbon scaffolds. *Mater Lett.* 2018;232:14-17.

93. Lao J, Dieudonné X, Bembakkar M, Jallot E. Bioactive glass coating on gelatin scaffolds at ambient temperature: easy route to make polymer scaffolds become bioactive. *J Mater Sci.* 2017;52:9129-9139.
94. Baino F. Bioactive glasses – When glass science and technology meet regenerative medicine. *Ceram Int.* 2018;44(13):14953-14966.
95. Chen QZ, Thompson ID, Boccaccini AR. 45S5 Bioglass®-derived glass-ceramic scaffolds for bone tissue engineering. *Biomaterials.* 2006;27(11):2414-2425.
96. Fu Q, Rahaman MN, Bal BS, Brown RF, Day DE. Mechanical and in vitro performance of 13–93 bioactive glass scaffolds prepared by a polymer foam replication technique. *Acta Biomater.* 2008;4:1854-1864.
97. Baino F, Vitale-Brovarone C. Mechanical properties and reliability of glass ceramic foam scaffolds for bone repair. *Mater Lett.* 2014;118:27-30.
98. Vitale-Brovarone C, Baino F, Tallia F, Gervasio C, Verné E. Bioactive glass-derived trabecular coating: a smart solution for enhancing osteointegration of prosthetic elements. *J Mater Sci Mater Med.* 2012;23:2369-2380.
99. Bretcanu O, Samaille C, Boccaccini AR. Simple methods to fabricate Bioglass®-derived glass-ceramic scaffolds exhibiting porosity gradient. *J Mater Sci.* 2008;43(12):4127-4134.
100. Baino F, Minguella J, Kirk N, Montealegre MA, Fiaschi C, Korkusuz F, et al. Novel full-ceramic monoblock acetabular cup with a bioactive trabecular coating: design, fabrication and characterization. *Ceram Int.* 2016;42:6833-6845.
101. Fukasawa T, Ando M, Ohji T, Kanzaki S. Synthesis of porous ceramics with complex pore structure by freeze-dry processing. *J Am Ceram Soc.* 2001;84:230-232.
102. Fukasawa T, Deng Z, Ando M, Ohji T, Kanzaki S. Synthesis of porous silicon

nitride with unidirectionally aligned channels using freeze-drying process. *J Am Ceram Soc.* 2002;85:2151-2155.

103. Deville S, Saiz E, Natta R, Tomsia A. Freezing as a path to build complex composites. *Science* (80- ). 2006;311:515-518.
104. Munch E, Launey ME, Alsem DH, Saiz E, Tomsia A, Ritchie R. Tough, bio-inspired hybrid materials. *Science* (80- ). 2008;322:1516-1520.
105. Fu Q, Rahaman MN, Bal BS, Brown RF. Preparation and in vitro evaluation of bioactive glass (13-93) scaffolds with oriented microstructures for repair and regeneration of load-bearing bones. *J Biomed Mater Res - Part A.* 2010;93(4):1380-1390.
106. Liu X, Rahaman MN, Fu Q, Tomsia AP. Porous and strong bioactive glass (13-93) scaffolds prepared by unidirectional freezing of camphene-based suspensions. *Acta Biomater.* 2012;8:415-423.
107. Minaberry Y, Jobbágy M. Macroporous bioglass scaffolds prepared by coupling sol-gel with freeze drying. *Chem Mater.* 2011;23(9):2327-2332.
108. Maquet V, Boccaccini AR, Pravata L, Notingher I, Jérôme R. Porous poly( $\alpha$ -hydroxyacid)/bioglass <sup>®</sup> composite scaffolds for bone tissue engineering. I: preparation and in vitro characterization. *Biomaterials.* 2004;25(18):4185-4194.
109. Thompson JD, Hench LL. Mechanical properties of bioactive glasses, glass-ceramics and composites. *Proc Inst Mech Eng H J Eng Med.* 1998;212:127-136.
110. Ding Y, Souza MT, Li W, Schubert DW, Boccaccini AR, Roether JA. Bioactive glass-biopolymer composites for applications in tissue engineering. In: Antoniac I . (Eds) *Handbook of Bioceramics and Composites.* Springer, Cham; 2016:325-356.
111. Niu Y, Guo L, Liu J, Shen H, Su J, An X, et al. Bioactive and degradable

scaffolds of the mesoporous bioglass and poly(L-lactide) composite for bone tissue regeneration. *J Mater Chem B*. 2015;3:2962-2970.

112. Bose S, Vahabzadeh S, Bandyopadhyay A. Bone tissue engineering using 3D printing. *Mater Today*. 2013;16(12):496-504.
113. Lee JW, Kim JY, Cho D-W. Solid free-form fabrication technology and its application to bone tissue engineering. *Int J stem cells*. 2010;3(2):85-95.
114. Gmeiner R, Deisinger U, Schönherr J, Lechner B, Detsch R, Boccaccini AR, et al. Additive manufacturing of bioactive glasses and silicate bioceramics. *J Ceram Sci Technol*. 2015;6(2):75-86.
115. Lorrison J, Goodridge R, Dalgarno K, Wood D. Selective laser sintering of bioactive glass-ceramics. *Proc 13th Ann Int Solid Free Fabr Symp*. 2002;1:1-8.
116. Shirazi SFS, Gharekhani S, Mehrali M, Yarmand H, Metselaar HSC, Adib Kadri N, et al. A review on powder-based additive manufacturing for tissue engineering: Selective laser sintering and inkjet 3D printing. *Sci Technol Adv Mater*. 2015;16(3).
117. Liu J, Hu H, Li P, Shuai C, Peng S. Fabrication and characterization of porous 45S5 glass scaffolds via direct selective laser sintering. *Mater Manuf Process*. 2013;28(6):610-615.
118. Gao C, Liu T, Shuai C, Peng S. Enhancement mechanisms of graphene in nano-58S bioactive glass scaffold: Mechanical and biological performance. *Sci Rep*. 2014;4.
119. Kolan KCR, Leu MC, Hilmas GE, Brown RF, Velez M. Fabrication of 13-93 bioactive glass scaffolds for bone tissue engineering using indirect selective laser sintering. *Biofabrication*. 2011;3(2).
120. Izquierdo-Barba I, Vallet-Regi M. Mesoporous bioactive glasses: relevance of

their porous structure compared to that of classical bioglasses. *Biomed Glas.* 2015;1:140-150.

121. Anselme K, Davidson P, Popa A, Giazzon M, Liley M, Ploux L. The interactions of cells and bacteria with surfaces structured at the nanometre scale. *Acta Biomater.* 2010;6:3824-3846.
122. Melchels FPW, Feijen J, Grijpma DW. A review on stereolithography and its applications in biomedical engineering. *Biomaterials.* 2010;31(24):6121-6130.
123. Tesavibul P, Felzmann R, Gruber S, Liska R, Thompson I, Boccaccini AR. Processing of 45S5 bioglass® by lithography-based additive manufacturing. *Mater Lett.* 2012;41:81-84.
124. Felzmann R, Gruber S, Mitteramskogler G, Tesavibul P, Boccaccini AR, Liska R, et al. Lithography- based additive manufacturing of cellular ceramic structures. *Adv Eng Mater.* 2012;14:1052-1058.
125. Thavornnyutikarn B, Chantarapanich N, Sitthiseripratip K, Thouas GA, Chen Q. Bone tissue engineering scaffolding: computer-aided scaffolding techniques. Vol 3.; 2014.
126. Li Z, Chen X, Zhao N, Dong H, Li Y, Lin C. Stiff macro-porous bioactive glass-ceramic scaffold: Fabrication by rapid prototyping template, characterization and in vitro bioactivity. *Mater Chem Phys.* 2013;141(1):76-80.
127. Mancuso E, Alharbi N, Bretcanu OA, Marshall M, Birch MA, McCaskie AW, et al. Three-dimensional printing of porous load-bearing bioceramic scaffolds. *Proc Inst Mech Eng Part H J Eng Med.* 2017;231(6):575-585.
128. Soundarya SP, Menon AH, Chandran SV, Selvamurugan N. Bone tissue engineering: Scaffold preparation using chitosan and other biomaterials with different design and fabrication techniques. *Int J Biol Macromol.* 2018;119:1228-1239.

129. Guvendiren M, Molde J, Soares RMD, Kohn J. Designing biomaterials for 3d printing. *ACS Biomater Sci Eng.* 2016;2(10):1679-1693.
130. Lewis JA, Smay JE, Stuecker J, Cesarano J. Direct ink writing of three-dimensional ceramic structures. *J Am Ceram Soc.* 2006;89(12):3599-3609.
131. Cesarano J. Robocasting of ceramics and composites using fine particle suspensions. United States: N. p., 1999. Web.
132. Lewis JA, Smay JE. Three-dimensional periodic structure. In: *Cellular ceramics: structure, manufacturing, properties and applications.* Wiley-VCH; 2005:87-100.
133. Carreau PJ, De Kee D, Daroux M. An analysis of the viscous behaviour of polymeric solutions. *Can J Chem Eng.* 1979;57:135-140.
134. Lewis JA. Direct-write assembly of ceramics from colloidal inks. *Curr Opin Solid State Mater Sci.* 2002;6(3):245-250.
135. Franco J, Hunger P, Launey ME, Tomsia AP, Saiz E. Direct write assembly of calcium phosphate scaffolds using a water-based hydrogel. *Acta Biomater.* 2010;6(1):218-228.
136. Fu Q, Saiz E, Tomsia AP. Direct ink writing of highly porous and strong glass scaffolds for load-bearing bone defects repair and regeneration. *Acta Biomater.* 2011;7(10):3547-3554.
137. Deliormanli AM, Rahaman MN. Direct-write assembly of silicate and borate bioactive glass scaffolds for bone repair. *J Eur Ceram Soc.* 2012;32(14):3637-3646.
138. Nommeots-Nomm A, Lee PD, Jones JR. Direct ink writing of highly bioactive glasses. *J Eur Ceram Soc.* 2018;38(3):837-844.
139. Motealleh A, Eqtesadi S, Civantos A, Pajares A, Miranda P. Robocast 45S5 bioglass scaffolds: in vitro behavior. *J Mater Sci.* 2017;52:9179-9191.

140. Mattioli-Belmonte M, De Maria C, Vitale-Brovarone C, Baino F, Dicarolo M, Vozzi G. Pressure-activated microsyringe (PAM) fabrication of bioactive glass/poly(lactic-co-glycolic acid) composite scaffolds for bone tissue regeneration. *J Tissue Eng Regen Med.* 2017;11:1986-1997.
141. Wu C, Chang J. Multifunctional mesoporous bioactive glasses for effective delivery of therapeutic ions and drug/growth factors. *J Control Release.* 2014;193:282-295.
142. Baino F, Fiorilli S, Vitale-Brovarone C. Bioactive glass-based materials with hierarchical porosity for medical applications: review of recent advances. *Acta Biomater.* 2016;42:18-32.
143. Wu C, Zhang Y, Zhu Y, Friis T, Xiao Y. Structure-property relationships of silk-modified mesoporous bioglass scaffolds. *Biomaterials.* 2010;31:3429-3438.
144. Garcia A, Izquierdo-Barba I, Colilla M, Laorden CL De, Vallet-Regí M. Preparation of 3-D scaffolds in the SiO<sub>2</sub>-P<sub>2</sub>O<sub>5</sub> system with tailored hierarchical meso-macroporosity. *Acta Biomater.* 2011;7:1265-1273.
145. Wu C, Luo Y, Cuniberti G, Xiao Y, Gelinsky M. Three-dimensional printing of hierarchical and tough mesoporous bioactive glass scaffolds with a controllable pore architecture, excellent mechanical strength and mineralization ability. *Acta Biomater.* 2011;7:2644-2650.
146. Zhang J, Zhao S, Zhu Y, Huang Y, Zhu M, Tao C, et al. Three-dimensional printing of strontium-containing mesoporous bioactive glass scaffolds for bone regeneration. *Acta Biomater.* 2014;10:2269-2281.
147. Ma H, Feng C, Chang J, Wu C. 3D-printed bioceramic scaffolds: from bone tissue engineering to tumor therapy. *Acta Biomater.* 2018;79:37-59.
148. Moroni L, Boland T, Burdick JA, De Maria C, Derby B, Forgacs G, et al.

Biofabrication: a guide to technology and terminology. *Trends Biotechnol.* 2018;36(4):384-402.

149. Groll J, Boland T, Blunk T, Burdick JA, Cho DW, Dalton PD, et al. Biofabrication: Reappraising the definition of an evolving field. *Biofabrication.* 2016;8(1).
150. Mironov V, Trusk T, Kasyanov V, Little S, Swaja R, Markwald R. Biofabrication: a 21st century manufacturing paradigm. *Biofabrication.* 2009;1:022001.
151. Jung J, Lee J, Cho D. Computer-aided multiple-head 3D printing system for printing of heterogeneous organ/tissue constructs. *Sci Rep.* 2016;6:21685.
152. Liverani L, Roether J, Noeaid P, Trombetta M, Schubert D, Boccaccini A. Simple fabrication technique for multilayered stratified composite scaffolds suitable for interface tissue engineering. *Mater Sci Eng A.* 2012;557:54-58.
153. Murphy C, Kolan K, Li W, Semon J, Day D, Leu M. 3D bioprinting of stem cells and polymer/bioactive glass composite scaffolds for tissue engineering. *Int J Bioprinting.* 2017;3(1).
154. Bairo F, Novajra G, Miguez-Pacheco V, Boccaccini A, Vitale-Brovarone C. Bioactive glasses: special applications outside the skeletal system. *J Non Cryst Solids.* 2016;452:15-30. Kargozar S, Hamzehlou S, Bairo F. Potential of bioactive glasses for cardiac and pulmonary tissue engineering. *Materials (Basel).* 2017;10:1429.
155. Hench LL. Glass and glass-ceramic technologies to transform the world. *Int J Appl Ceram Sci.* 2011:162-176.

## Figures captions

**Figure 1.** Porosity vs. compressive strength of different glass scaffold compared with the human bone. Gray: sol-gel; green: freeze casting; pink: thermally bonded particles; purple: solid free-form fabrication; blue: polymer foam replication. Adapted from [16].

**Figure 2.** Driving force effects: coarsening without pores removal and densification [57].

**Figure 3.** Scheme of spherical grains bonded by a neck with description and effects of the different diffusion mechanisms [58].

**Figure 4.** Scaffolds produced by foaming methods: tomographic reconstruction of a melt-derived bioactive glass scaffold produced by gel-cast foaming [67] (a); bubble-like typical morphology of a scaffold with composition 70S30C obtained by sol-gel foaming and thermally stabilized at 600 °C [46] (b); SEM image of the inner structure of a scaffold produced by in situ foaming [74] (c); the macrostructure of a glass scaffold foamed by H<sub>2</sub>O<sub>2</sub> [75] (d).

**Figure 5.** 13-93 glass scaffold mimicking a tibial plate: surface morphology after sintering (a) and general view (b). The different particles are clearly distinguishable in (a) with the sintering necks that are bridging them. Adapted from [76].

**Figure 6.** SEM micrographs of macroporous scaffolds produced by using several polymeric fillers as porogen particles: porous bioactive ceramic scaffold prior to surface modification with macro-pores ranging between 200-300 μm produced by using camphor as sacrificial

pores template [79] (a); SEM micrographs of a macro-porous glass-ceramic scaffold obtained by using PE particles (200-300  $\mu\text{m}$ ) as pores forming agent [80] (b); SEM micrograph of a glass-ceramic scaffold obtained using potato starch as pore-generating agent [83] (c); elongated pores in a scaffold obtained by rice husk burning-out [86] (d).

**Figure 7.** Scaffold fabricated by replication approaches: examples of bioactive glass coatings on poly(DL-lactide) biodegradable polymeric foams [87] (a) and wood-derived carbon scaffolds [92] (b) obtained by slurry dipping technique; 45S5 Bioglass<sup>®</sup> foam with details of the trabecular structure (c) and the hollow structure of a trabecula (d) [95].

**Figure 8.** 3D pore-graded 45S5 Bioglass<sup>®</sup> scaffold obtained by pre-forming a PU foam [99].

**Figure 9.** Processing steps of a porous polymeric scaffold by SCPL. The addition of ceramic or glass particles to produce a composite scaffold should occur before step A but is not reported in this scheme [110].

**Figure 10.** Working scheme of a SLS machine [116].

**Figure 11.** Two different kinds of SLA: Right: top-down approach; Left: DLP bottom-up approach [122].

**Figure 12.** 45S5 Bioglass<sup>®</sup> scaffolds produced by SLA having (a) an ordered pore/strut architecture or (b) trabecular structure being generated from micro-tomographic images of human femoral bone. Images adapted from Tesavibul *et al.* [123]; Gmeiner *et al.* [114].

**Figure 13.** Indirect SLA-based method: (a) CAD model of the polymeric template; (b)  $\mu$ -CT image of the 45S5 Bioglass<sup>®</sup>-derived glass-ceramic scaffold; (c) SEM micrograph of the pore/strut structure [126].

**Figure 14.** Steps of a 3DP process, from left, clockwise: formation of the new layer on the powder bed; jetting of the binder; lowering of the building bed; extraction of the green body. The first three steps are repeated as many times as needed [114].

**Figure 15.** Robocasting of MBG scaffolds: (A) sol-gel-based synthesis of MBGs with ordered meso-pores; (B) 3DP of MBG scaffolds exhibiting three scales of porosity: ultra-large pores, macro-pores, and meso-pores. Images reproduced from [144].

**Figure 16.** The experimental set-up used for the robocasting of bioactive glass scaffolds (photo courtesy of Jacopo Barberi and Jonathan Massera, 2018, Tampere University, Tampere, Finland).

**Figure 17.** SEM micrographs of 45S5 glass-derived robocast scaffolds: (a) overview of the green structure; single rod images of scaffolds sintered at (b) 550 °C and (c) 1000 °C [139].

**Figure 18.** SEM morphological analysis of chitosan-based samples before (a-b) and after (c-d) bioactivity tests in Simulated Body Fluid (SBF) [152].

## Tables

**Table 1.** Overview of the key properties for a scaffold aimed at regenerating bone (adapted from [48]).

<i>Property</i>	<i>Effect/explanation</i>
<b><i>Ability to deliver cells</i></b>	The material should not only be biocompatible (i.e. harmless) but also foster cell attachment, differentiation, and proliferation.
<b><i>Osteoconductivity</i></b>	It would be best if the material encourages osteoconduction with host bone. Osteoconductivity does not only eliminate the formation of fibrous tissue encapsulation but it also brings about a strong bone between the scaffold and host bone.
<b><i>Biodegradability</i></b>	The composition of the material, combined with the porous structure of the scaffold, should lead biodegradation <i>in vivo</i> at rates appropriate to tissue regeneration.
<b><i>Mechanical properties</i></b>	The mechanical strength of the scaffold, which is determined by both the properties of the biomaterial and the porous structure, should be sufficient to provide mechanical stability to constructs in load-bearing sites prior to synthesis of the new extracellular matrix (ECM) by cells.
<b><i>Porous structure</i></b>	The scaffold should have an interconnected porous structure with porosity > 90% and diameters between 300-500 $\mu\text{m}$ for cell penetration, tissue ingrowth and vascularization and nutrient delivery.
<b><i>Fabrication</i></b>	The material should possess desired fabrication capability, e.g. being readily produced into irregular shapes of scaffolds that match the defects in the bone of individual patients.
<b><i>Commercialization potential</i></b>	The synthesis of the material and fabrication of the scaffold should be reproducibly suitable for commercialization. The scaffold should also be sterilizable and accessible at a reasonable cost.

**Table 2.** Overview of the manufacturing techniques used for the production of glass-based scaffolds in bone tissue engineering.

<i>Major group</i>	<i>Technological class</i>	<i>Specific methods</i>
<b>Conventional</b>	Foaming techniques	Gel-casting foaming, sol-gel foaming, H <sub>2</sub> O <sub>2</sub> foaming
	Thermal consolidation of particles	Organic phase burning out: polymeric porogens, starch consolidation, rice husk method
	Porous polymer replication	Coating methods, foam replication
	Freeze-drying	Freeze casting of suspensions, ice-segregation-induced self-assembly (ISISA)
	Thermally induced phase separation (TIPS)	
	Solvent-casting and particulate leaching (SCPL)	
<b>Additive manufacturing</b>	Selective laser sintering (SLS)	
	Stereolithography (SLA)	
	Direct ink writing	3D printing, ink-jet printing, robocasting

**Table 3.** Overview of material flow mechanisms, material sources, relevant effects and parameters involved (adapted from [57], [58]).

<i>Diffusion mechanism</i>	<i>Material source</i>	<i>Effect</i>	<i>Parameters</i>
- <b>Surface diffusion</b>	Grain surface	Consolidation	Surface diffusivity
- <b>Lattice diffusion</b>	Grain surface	Consolidation	Lattice diffusivity
- <b>Vapor transport:</b>			
<i>Evaporation/condensation</i>	Grain surface	Consolidation	Difference in vapor pressure
<i>Gas diffusion</i>			Gas diffusivity
- <b>Grain boundary diffusion</b>	Grain boundary	Densification	Grain boundary diffusivity
- <b>Lattice diffusion</b>	Grain boundary	Densification	Lattice diffusivity
- <b>Plastic flow</b>	Bulk	Densification	Viscosity

**Table 4.** Overview of AMTs employed for bone tissue engineering along with materials used, advantages and disadvantages of the single techniques. Adapted from Bose *et al.* [112].

<i>Technique</i>	<i>Process details</i>	<i>Materials for Bone Tissue Engineering</i>	<i>Advantages (+) and disadvantages (-)</i>	<i>Refereces</i>
<b>SLS</b>	<ul style="list-style-type: none"> <li>- Preparing the powder bed</li> <li>- Layer by layer addition of powder</li> <li>- Sintering each layer according to the CAD file, using a laser source</li> </ul>	<ul style="list-style-type: none"> <li>- PCL</li> <li>- Nano HA</li> <li>- CaP/PHBV</li> <li>- CHAp/PLLA</li> <li>- PLLA</li> <li>- B-TCP</li> <li>- PHBV</li> </ul>	<ul style="list-style-type: none"> <li>(+) No need for support</li> <li>(+) No post-processing</li> <li>(-) Feature resolution depends on laser beam diameter</li> </ul>	[114-120]
<b>SLA</b>	<ul style="list-style-type: none"> <li>- Immersion of platform in photopolymer liquid</li> <li>- Exposure to focused light according to the desired design</li> <li>- Polymer solidifying at the focal point, non-exposed polymer remains liquid</li> <li>- Layer by layer fabrication by platform moving downward</li> </ul>	<ul style="list-style-type: none"> <li>- PPF/DEF</li> <li>- PPF/DEF-HA</li> <li>- PDLLA/HA</li> <li>- B-TCP</li> </ul>	<ul style="list-style-type: none"> <li>(+) Complex internal features can be obtained</li> <li>(+) Growth factors, proteins, and cell patterning is possible</li> <li>(-) Only applicable for photopolymers</li> </ul>	[122-126]
<b>FDM</b>	<ul style="list-style-type: none"> <li>- Strands of heated polymer/ceramics extrusion through a nozzle</li> </ul>	<ul style="list-style-type: none"> <li>- TCP</li> <li>- TCP/PP</li> <li>- Al<sub>2</sub>O<sub>3</sub></li> <li>- PCL</li> <li>- TCP/PCL</li> </ul>	<ul style="list-style-type: none"> <li>(+) No need for platform/support</li> <li>(-) Materials restriction due to the need for molten phase</li> </ul>	[114]
<b>Laser-assisted bioprinting (LAB)</b>	<ul style="list-style-type: none"> <li>- Coating the desired material on transparent quartz disk (ribbon)</li> <li>- Deposition control by laser pulse energy</li> <li>- Resolution control by the distance between ribbon/substrate, spot size, and stage movement</li> </ul>	<ul style="list-style-type: none"> <li>- HA</li> <li>- Zirconia</li> <li>- HA/MG63</li> <li>- Nano HA</li> <li>- Human osteoprogenitor cell</li> <li>- Human umbilical vein endothelial cell</li> </ul>	<ul style="list-style-type: none"> <li>(+) Ambient condition</li> <li>(+) Applicable for organic, inorganic materials and cells</li> <li>(+) Quantitatively controlled</li> <li>(+) 3D stage movement</li> <li>(-) Homogeneous ribbon needed</li> </ul>	[148-156]

**3D plotting / direct ink writing**

- Strands of paste/viscous material (in solution form) extrusion based on the predesigned structure
- Layer by layer deposition of strands at a constant rate, under specific pressure
- Disruption of strands according to the tear of speed

- PCL
- HA
- Bioactive glasses
- Mesoporous bioactive glass/alginate composite
- PLA/PEG
- PLA/(PEG)/G5 glass
- PHMGCL Bioactive 6P538 glass
- HA/PLA
- HA/PCL
- 6P53B glass/PCL

(+) mild condition of the process allows drug and biomolecules plotting

[114,127]

**Robotic-assisted deposition/robocasting**

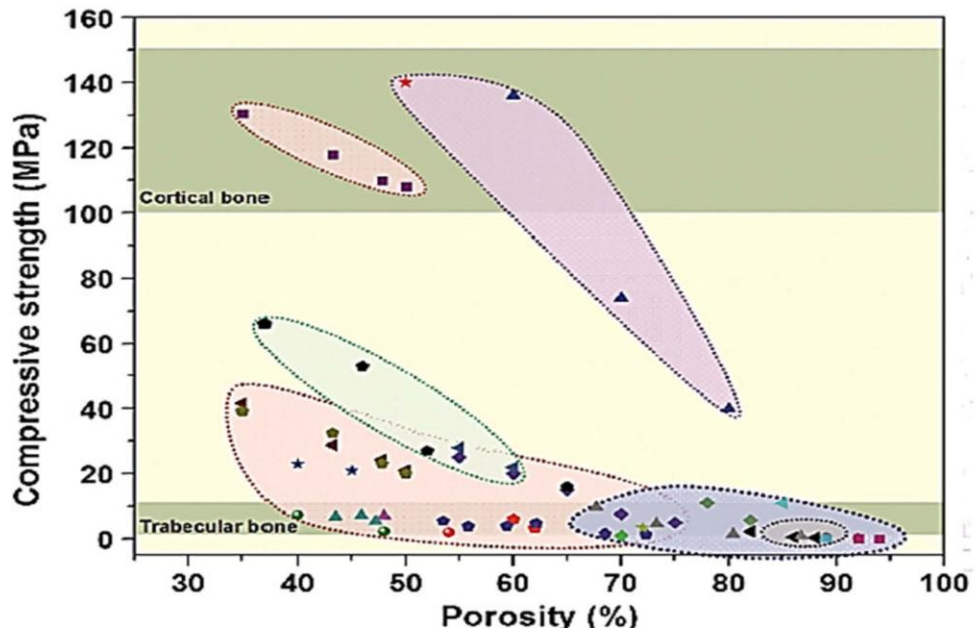
- Direct writing of liquid using a nozzle
- Consolidation through the liquid-to-gel transition

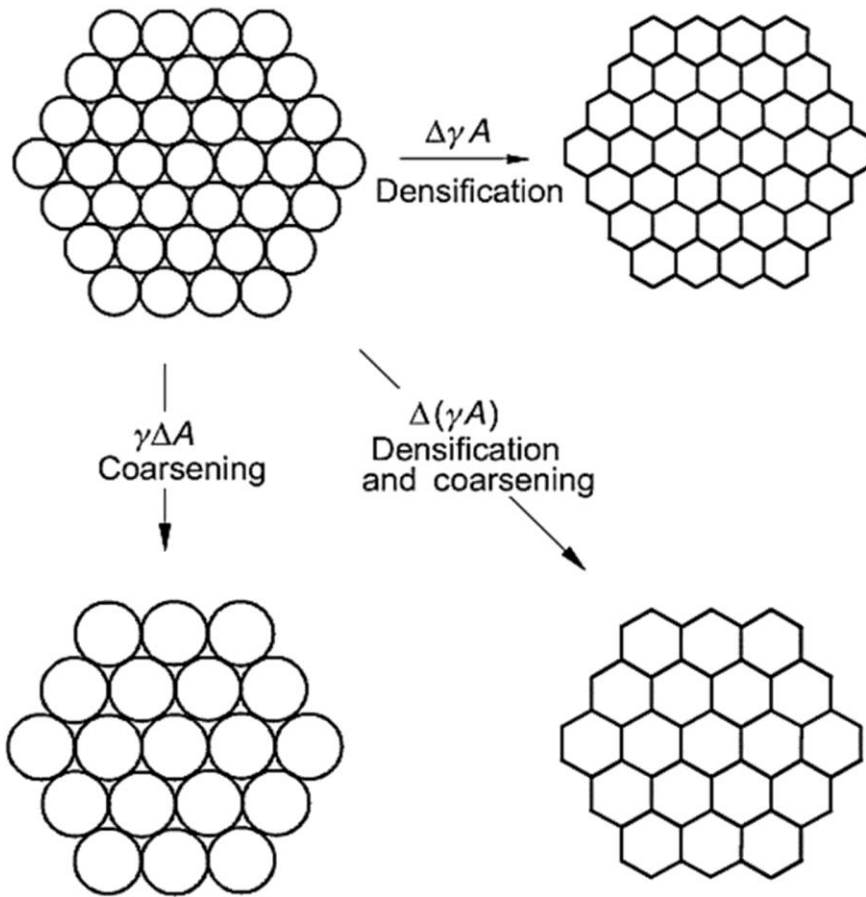
(-) Heating/post-processing needed for some materials restricts the biomolecule incorporation

[135-147]

(+) Independent 3D nozzle movement  
 (+) Precise control of the thickness  
 (+) No need for platform-support

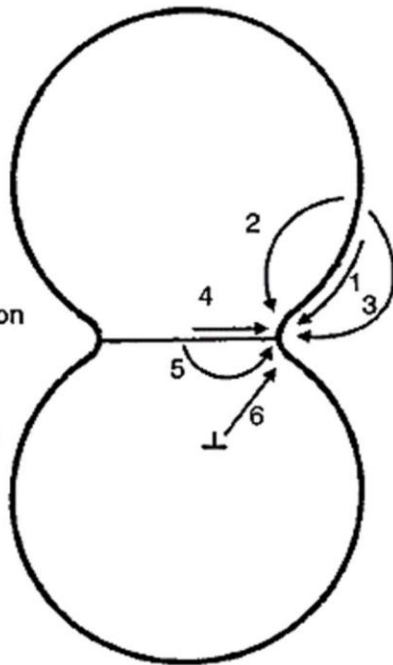
(-) Material restriction





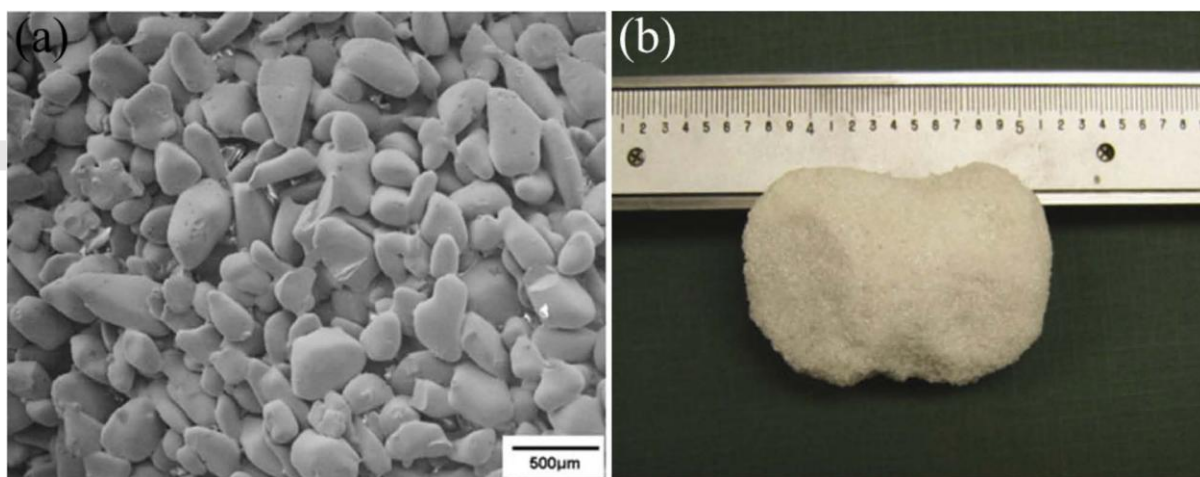
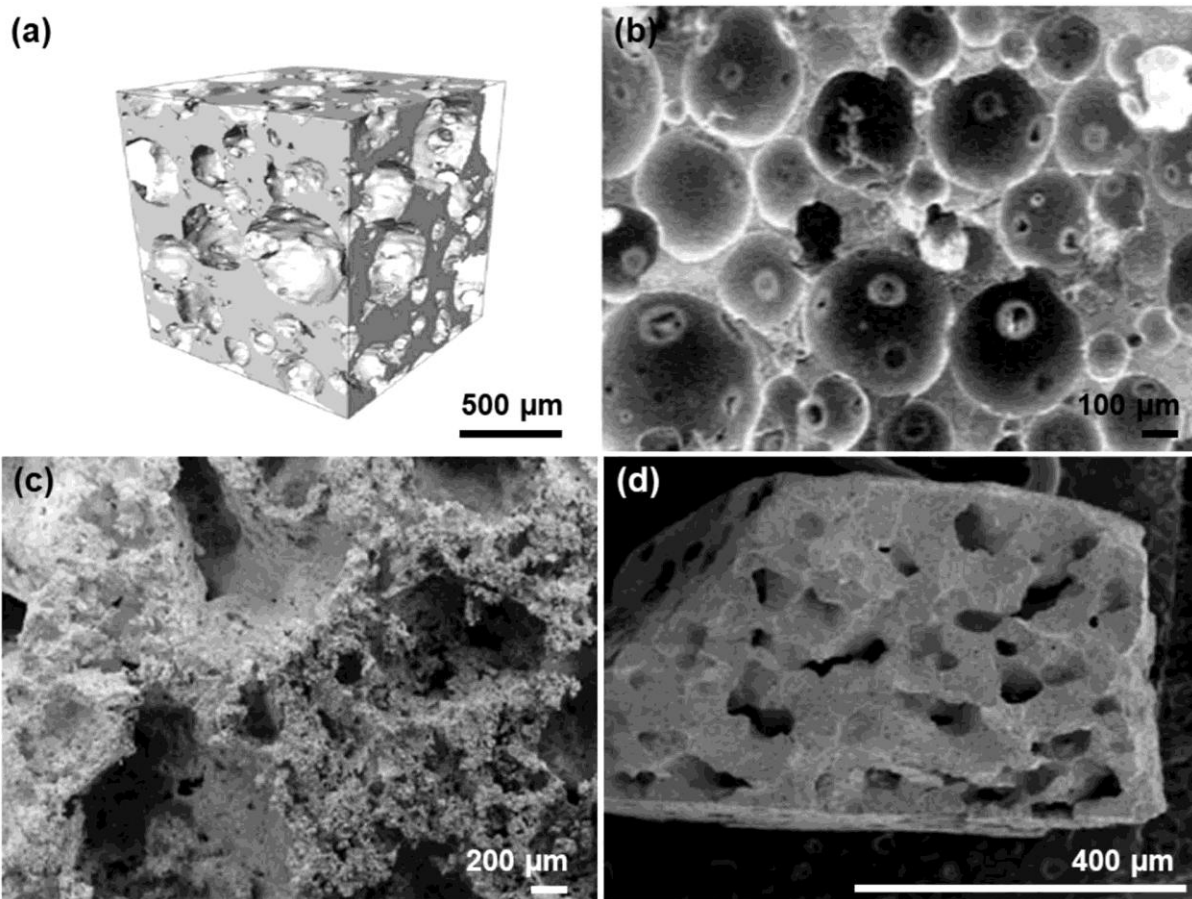
**Mechanisms**

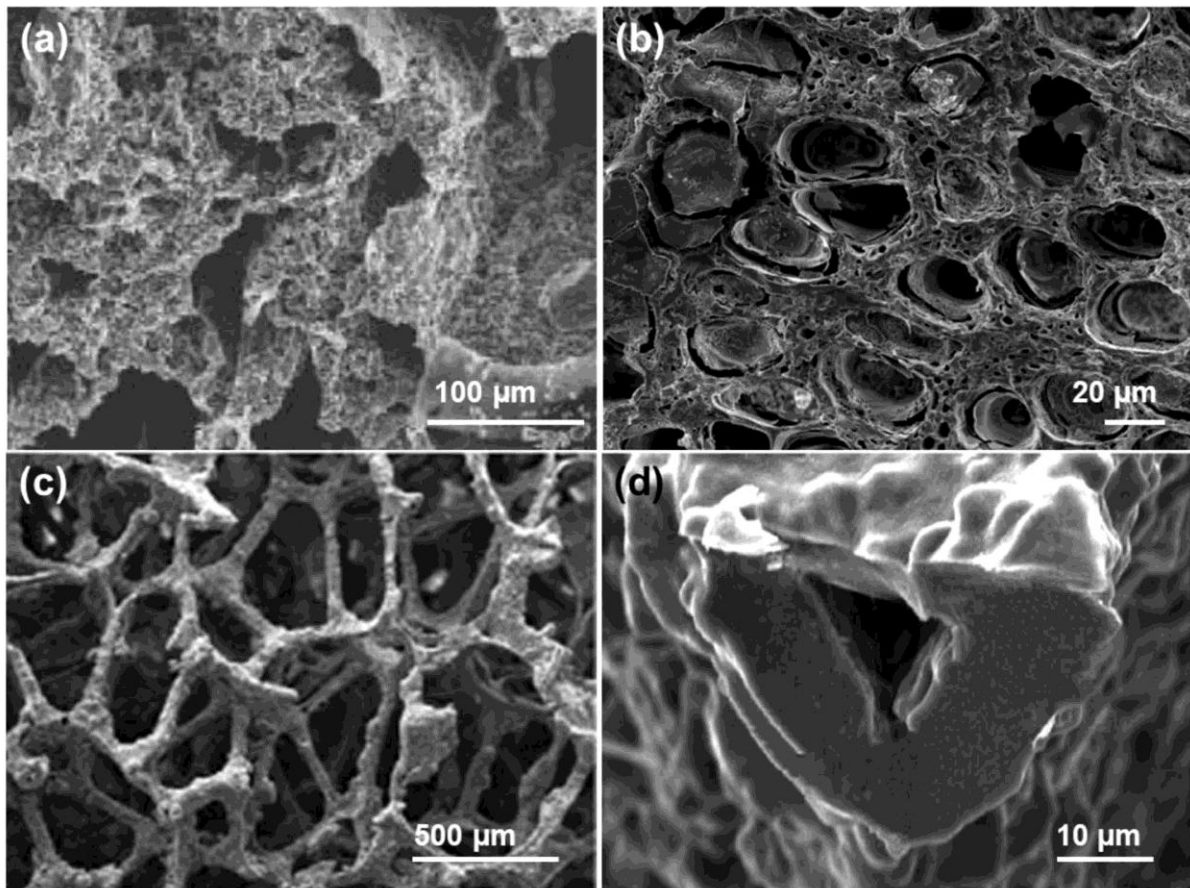
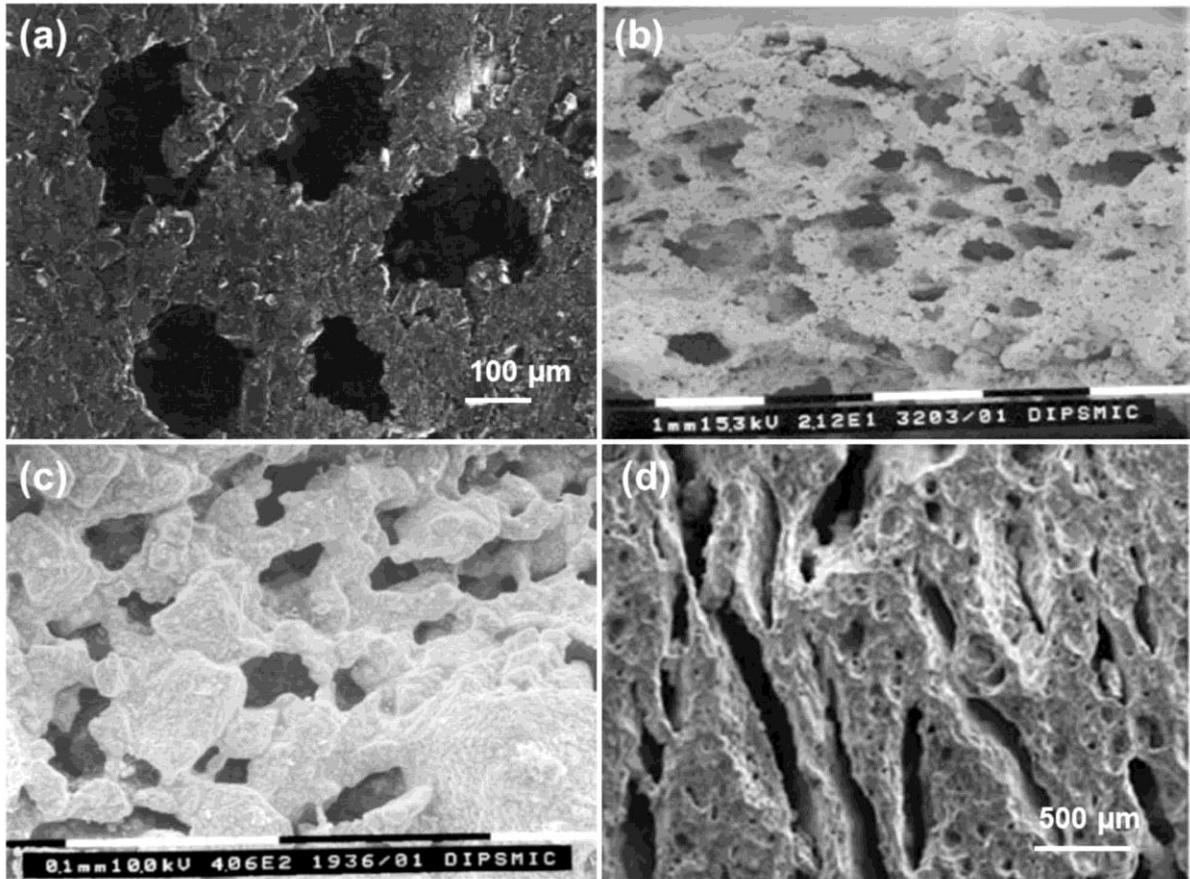
1. Surface diffusion
2. Lattice diffusion (from the surface)
3. Vapor transport
4. Grain boundary diffusion
5. Lattice diffusion (from the grain boundary)
6. Plastic flow (by dislocation motion)

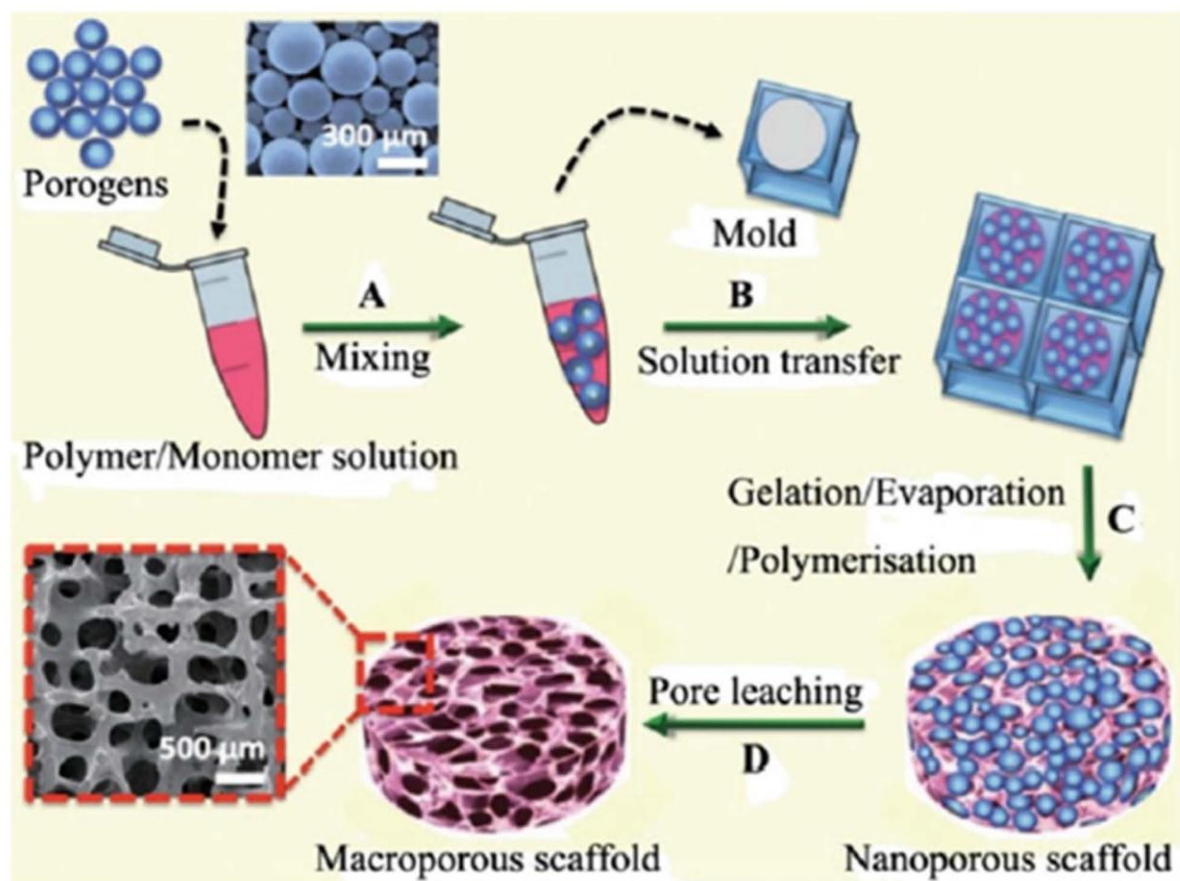
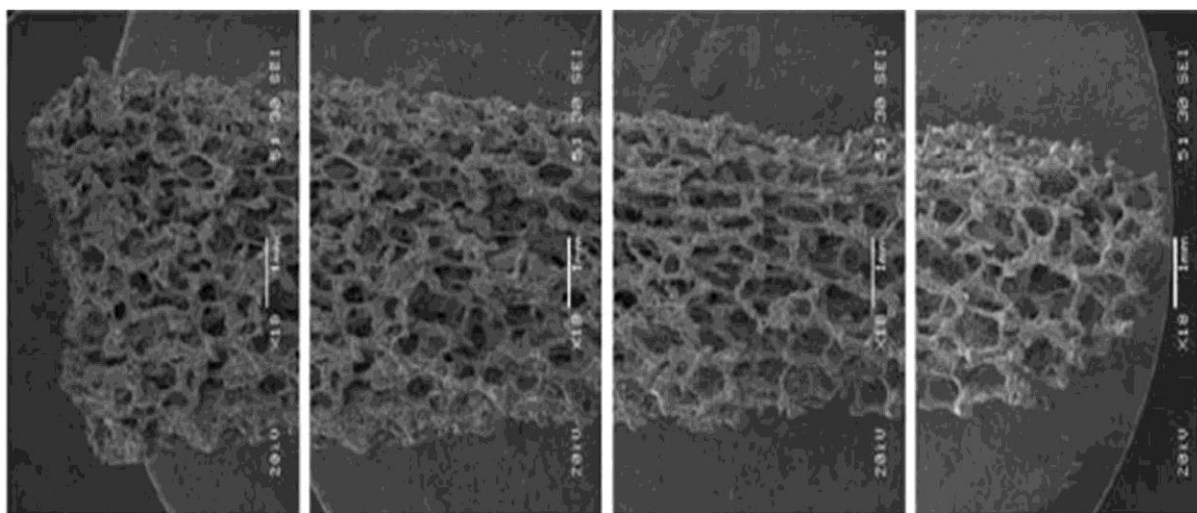


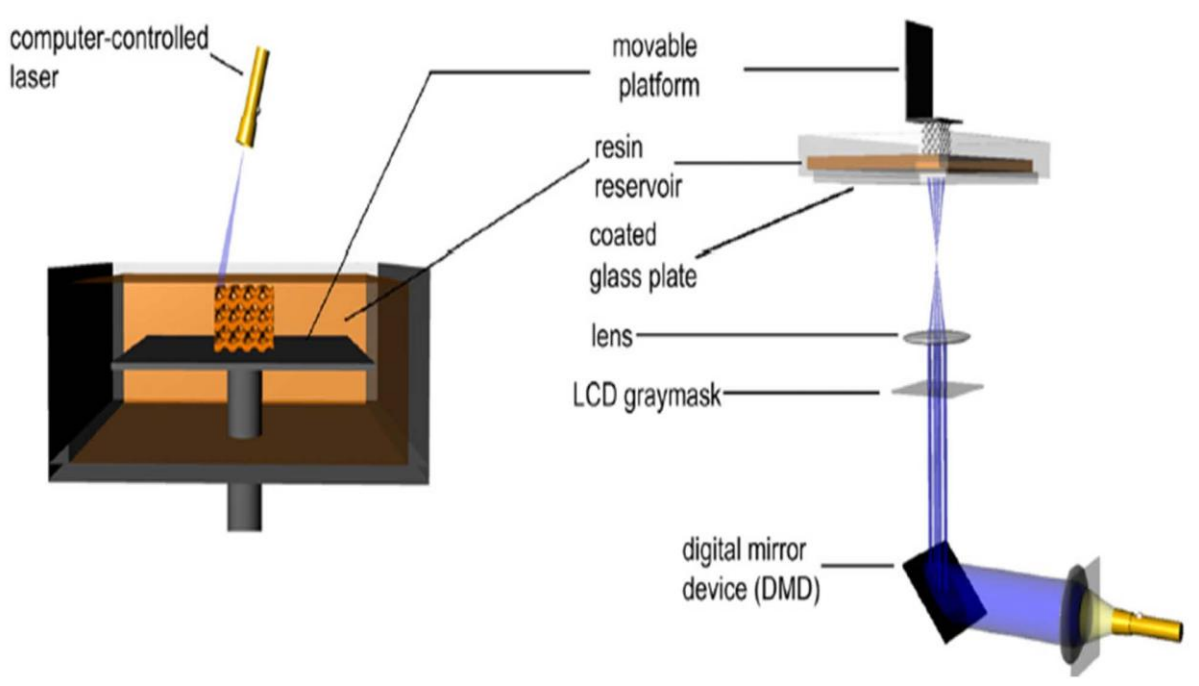
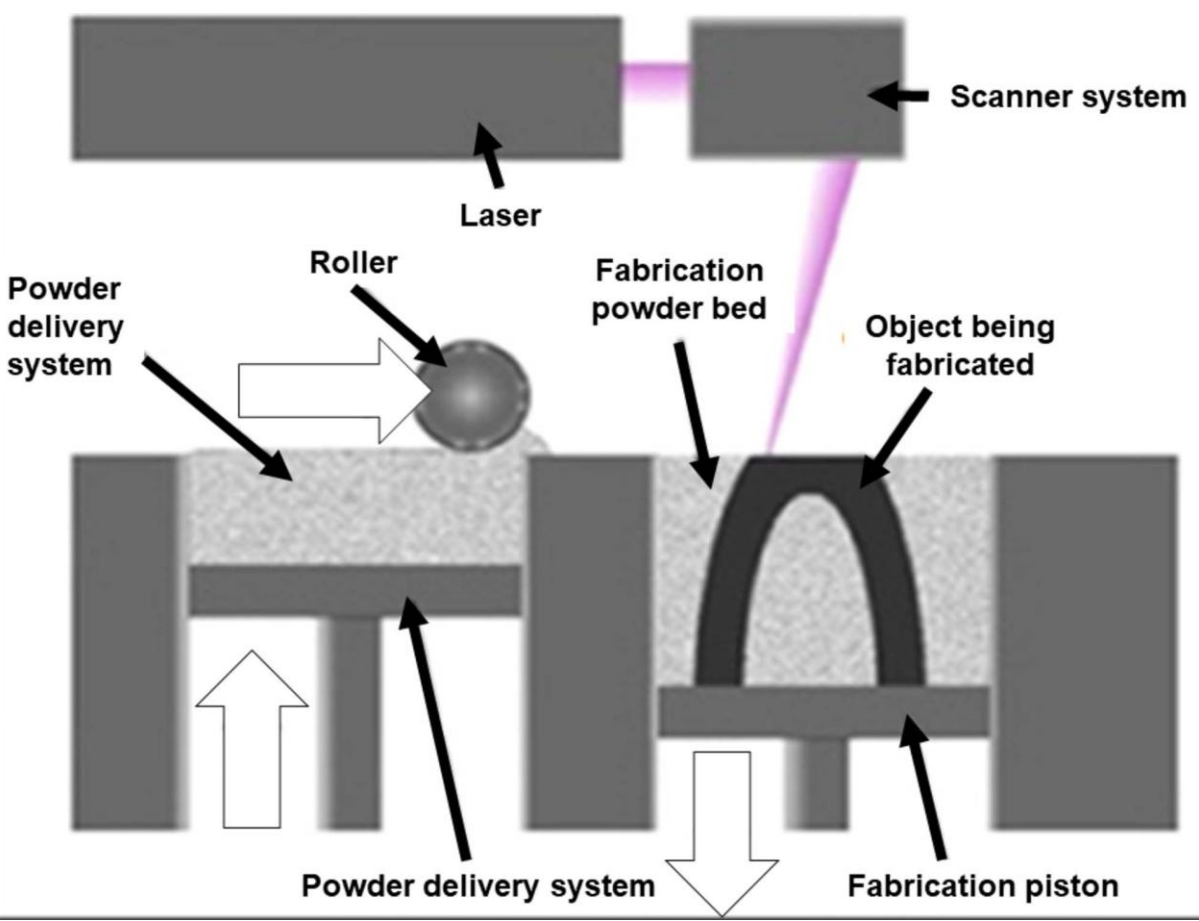
*Non-densifying mechanisms 1, 2, and 3 produce microstructural change without causing shrinkage*

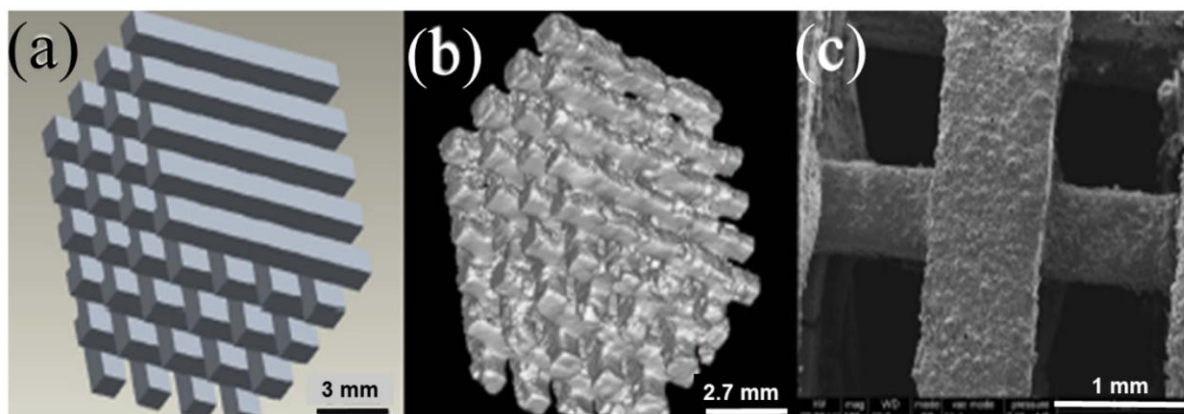
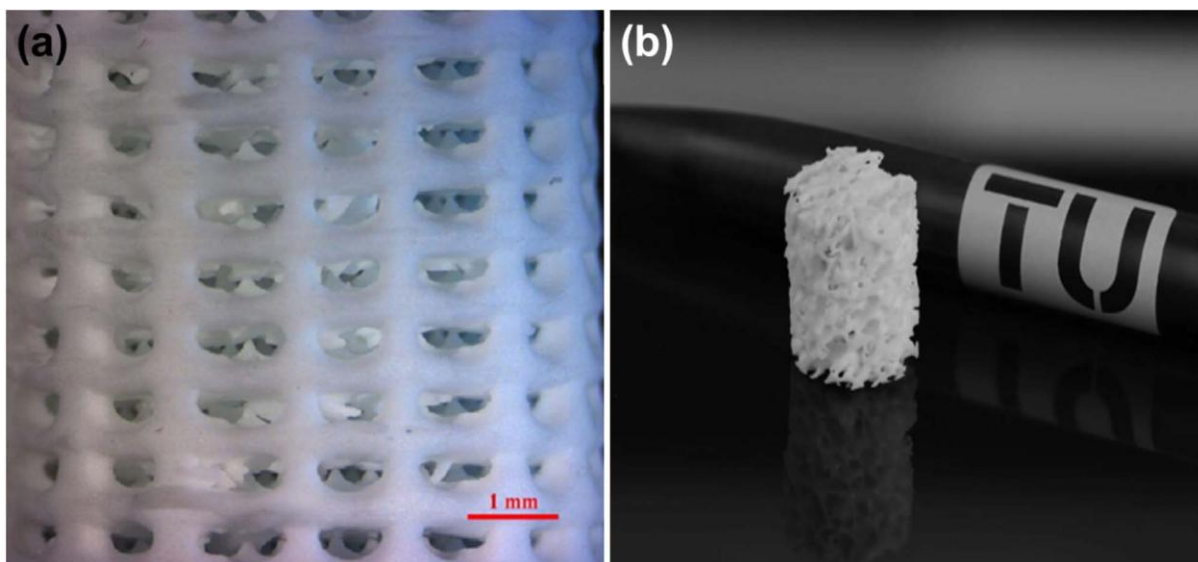
*Densifying mechanisms 4, 5, and 6 remove material from the grain boundary region leading to shrinkage*

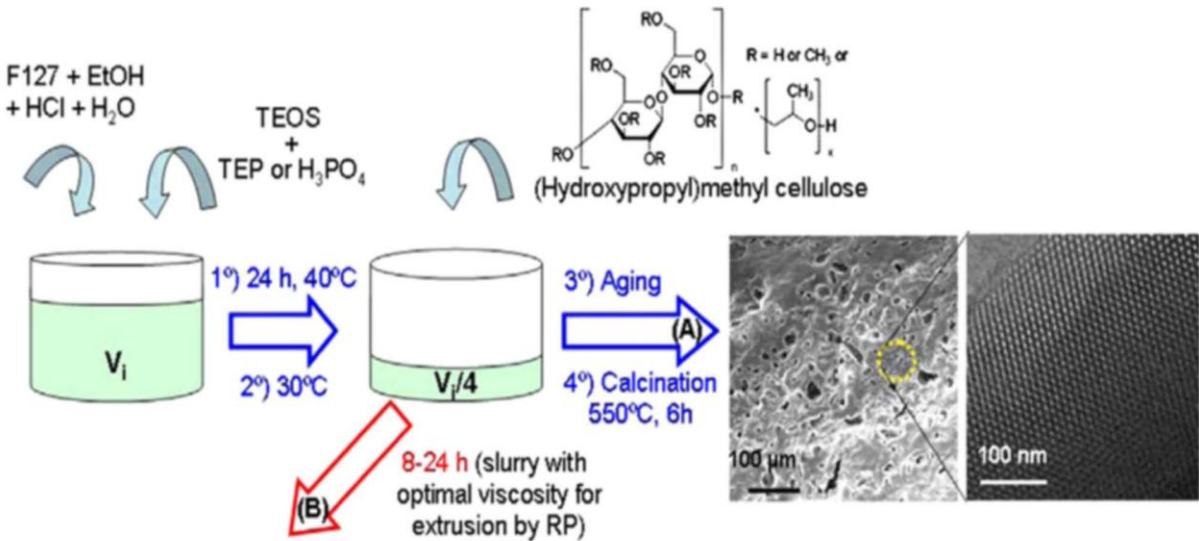
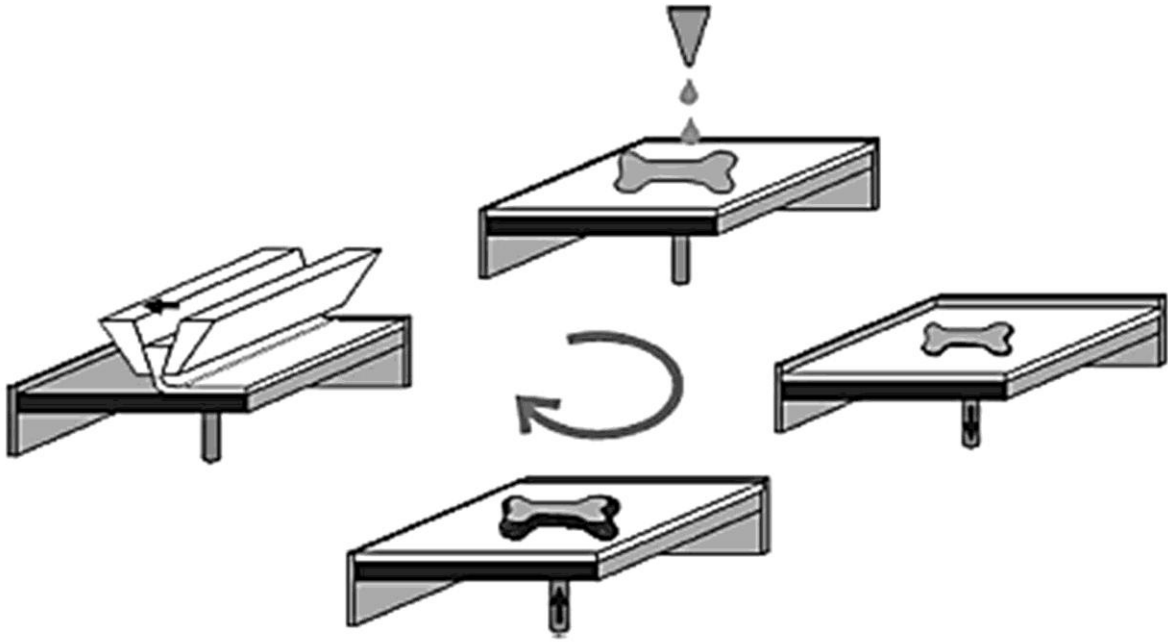












3° Rapid Prototyping (RP)

